1 # Bacteriophages targeting *Acinetobacter baumannii* capsule

2 # induce antimicrobial resensitization

3

4 Fernando Gordillo Altamirano[1]*, John H. Forsyth[1], Ruzeen Patwa[1], Xenia Kostoulias[2], Michael Trim[1], Dinesh

5 Subedi[1], Stuart Archer[3], Faye C. Morris[2], Cody Oliveira[1], Luisa Kielty[1], Denis Korneev[1], Moira K. O'Bryan[1],

6 Trevor J. Lithgow[2], Anton Y. Peleg[2,4], Jeremy J. Barr[1]*

7

8 [1] School of Biological Sciences, Monash University

9 [2] Biomedicine Discovery Institute and Department of Microbiology, Monash University

10 [3] Monash Bioinformatics Platform, Faculty of Medicine, Nursing and Health Sciences, Monash University

11 [4] Department of Infectious Diseases, The Alfred Hospital and Central Clinical School, Monash University

12

13 *Corresponding authors

14 Fernando Gordillo Altamirano   fernando.gordilloaltamirano@monash.edu

15 Jeremy J. Barr   jeremy.barr@monash.edu

16   School of Biological Sciences, Monash University

17   25 Rainforest Walk,

18   Clayton, 3800, VIC

19   Australia

20

21 ## Abstract

22 Carbapenem-resistant *Acinetobacter baumannii* is responsible for frequent, hard-to-treat and often fatal

23 healthcare-associated infections. Phage therapy, the use of viruses that infect and kill bacteria, is an approach

24 gaining significant clinical interest to combat antibiotic-resistant infections. However, a major limitation is that

25 bacteria can develop resistance against phages. Here, we isolated phages with activity against a panel of *A.*

26 *baumannii* strains and focused on clinical isolates AB900 and A9844 and their phages for detailed

27 characterization. As expected, coincubation of the phages with their hosts *in vitro* resulted in the emergence of

28 phage-resistant bacterial mutants. Genome sequence analysis revealed that phage-resistant mutants harbored

29 loss-of-function mutations in genes from the K locus, responsible for the biosynthesis of the bacterial capsule.

30 Using molecular biology techniques, phage adsorption assays, and quantitative evaluation of capsule

31 production, we established that the bacterial capsule serves as the primary receptor for these phages. As a

32 collateral phenotype of impaired capsule production, the phage-resistant strains could not form biofilms, became

33 fully sensitized to the human complement system, showed increased susceptibility to beta-lactam antibiotics,

34 and became vulnerable to additional phages. Finally, in a murine model of bacteremia, the phage-resistant *A.*

35 *baumannii* demonstrated a diminished capacity to colonize blood and solid tissues. This study demonstrates

36 that phages can be used not only for their lytic activity but, if combined with *a posteriori* knowledge of their

37 receptors and the mechanism of bacterial resistance, for their potential synergy with other antimicrobial agents,

38 thus providing even broader clinical options for phage therapy.

39

40 ## Keywords

41 Phage therapy, *Acinetobacter baumannii,* bacterial capsule, phage receptors, antimicrobial resistance.

42

Introduction

In 2019, antimicrobial resistance was listed by the World Health Organization (WHO) as one of the top ten threats to global health (1). Multidrug resistant (MDR) infections are consistently associated with poor clinical outcomes and represent a significant financial burden on the healthcare system (2, 3). Also in 2019, the WHO and Centers for Disease Control and Prevention (CDC) prioritized carbapenem-resistant *Acinetobacter baumannii* as a pathogen critically requiring research and development of new antimicrobial strategies (4, 5). *A. baumannii*, a gram-negative coccobacillus, is a member of the *ESKAPE* group of pathogens, which are prominent for causing frequent and hard-to-treat healthcare-associated infections (6).

As a species, *A. baumannii* is highly resilient, and capable of surviving for months in biofilms on abiotic surfaces (7, 8). It can cause pneumonia, bacteremia, urinary tract infections, meningitis and wound infections, particularly in the context of intensive care units, and is frequently associated with indwelling medical devices (8). Previous studies have estimated *A. baumannii* to be the causative agent of up to 20% of infections within intensive care units worldwide (9). The pathogenicity of *A. baumannii* is facilitated by features of the bacterial cell surface, including secretion of an extracellular polysaccharide capsule, outer membrane proteome, and iron acquisition systems (10, 11). The extracellular capsule is of particular importance, given that it is an essential feature for biofilm formation (12), which in turn protects *A. baumannii* from the immune system, antibiotics and disinfectants (13, 14), and increases the risk of co-colonization with other pathogens (15). The capsule also allows the pathogen to escape the action of antibodies and complement-mediated killing, promotes intrinsic antimicrobial-resistant phenotypes, and increases virulence (16).

Bacteriophages (phages) are viruses that infect and kill bacteria, making them an attractive option to combat antimicrobial resistance (17). Phage therapy is the administration of phages directly to a patient with the purpose of lysing the underlying bacterial pathogen (18). Since phages are highly species-specific, phage therapy has a favorable safety profile and does not disturb the microbiome in the way antibiotics do. However, this also means that both diagnosis of the infection and identification of the etiological agent are required to generate a precise phage-host match that will maximize treatment effectiveness (17). Under these circumstances, it is useful to establish and expand collections of well-characterized phages against problematic pathogens such as *A. baumannii*. Phage therapy has shown promising results against *A. baumannii* in murine models of pneumonia (19), bacteremia (20) and wound infections (21). And in 2017, the first case of successful intravenous and intracavitary phage therapy targeting a systemic MDR infection was reported in the United States (22), involving a 68-year-old diabetic patient with necrotizing pancreatitis complicated by an MDR *A. baumannii* infection that was treated with successive administration of phage cocktails (22).

Phage specificity is regarded as a major limitation to making phage therapy more accessible. The primary determinant for phage specificity occurs during the first step of the phage infection cycle, which is the adsorption of the phage to its receptor on the bacterial cell surface. In the case of *A. baumannii*, the cell surface comprises a range of structures composed both of proteins and polysaccharides (11). The first layer of this cell surface are the capsular polysaccharides and, in *A. baumannii*, more than forty distinct capsular polysaccharide structures have been chemically determined and more than a hundred diverse capsule types predicted based on genome sequence analysis (16, 23). Likewise, the outer membrane proteome in *A. baumannii* can vary greatly from strain to strain (11). Given that there is a current lack of serotyping to provide information on the capsule-type of *A. baumannii* clinical isolates, experimentally determining a precise host-phage match is an important issue.

2

84   Bacteria rapidly adapt to external pressures and can evolve resistance to antibiotics and phages alike.
85   Lytic phages impart strong selective pressures on their hosts, and phage-resistant phenotypes can emerge in
86   clinically-relevant timeframes (24). In particular, *in vitro* phage resistance often arises through the modification
87   or loss of surface receptors used during phage adsorption (25). This can result in the loss of the physiological
88   function of the receptor, with a collateral reduction in bacterial fitness, often referred to as a 'trade-off' (26, 27).
89   Trade-offs have been documented in various species and include decreased growth and impaired production
90   of capsules in *Staphylococcus aureus* (28), loss of virulence in *Salmonella enterica* (29), and resensitization to
91   antibiotics in *Pseudomonas aeruginosa* (30). Understanding phage-resistance mechanisms and their
92   associated trade-offs can allow for their clinical exploitation, opening the door to the next generation of phage
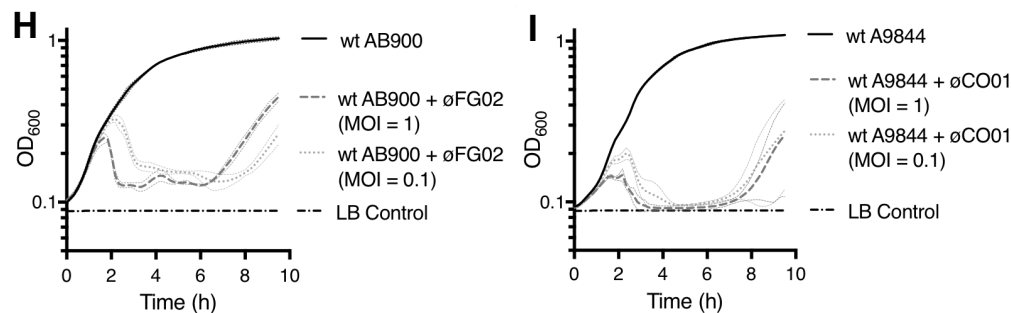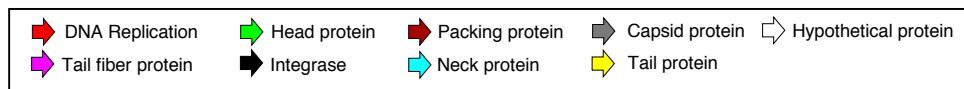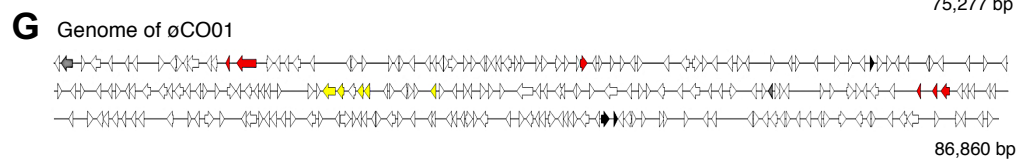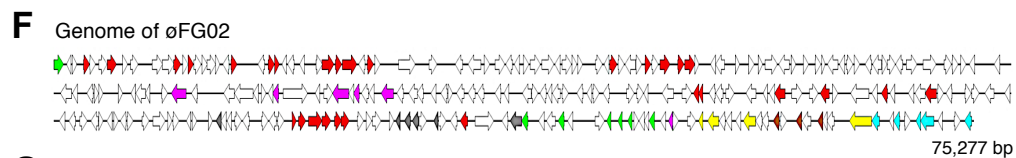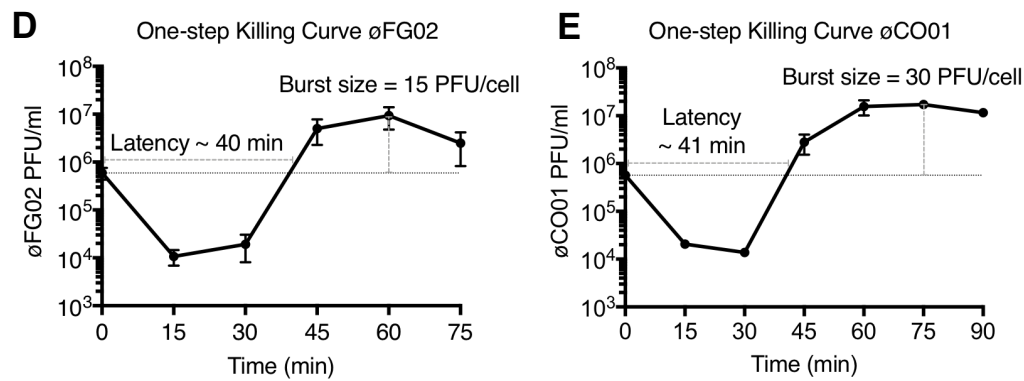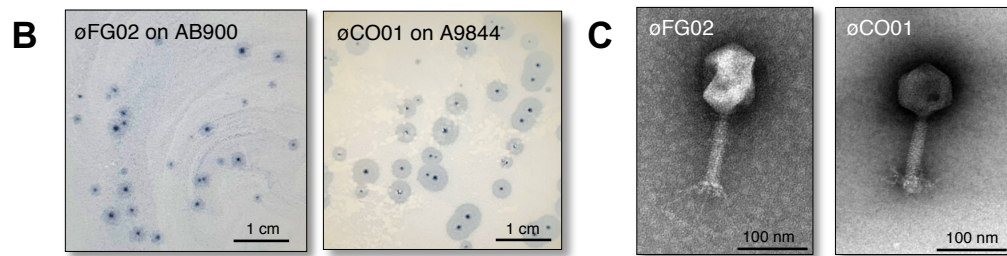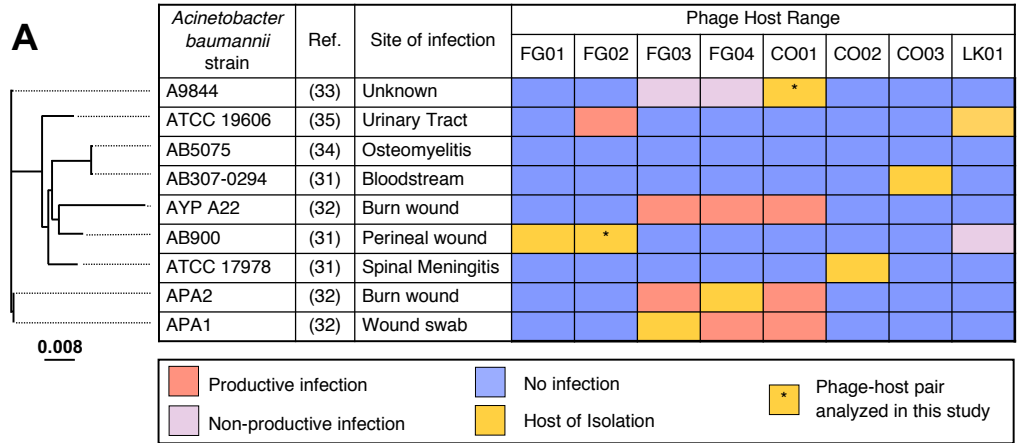93   therapy.

94   In this study, we isolated and characterized novel phages active against clinical isolates of *A.*
95   *baumannii*, including carbapenem-resistant isolates, to establish a phage library against this species. Upon
96   examination of lytic phage activity, we observed that phage-resistant mutants quickly emerged *in vitro*. Using
97   next-generation sequencing and bacterial genomics, we identified mutations in the genes associated with
98   capsule production and confirmed that they were causative for the phage-resistant phenotypes. We used
99   genetic engineering and phage adsorption assays to identify the capsule of *A. baumannii* as the primary phage
100 receptor, and established that phage-resistance emerged through loss of this receptor and subsequent lack of
101 phage adsorption. As a result, phage-resistant mutants exhibited altered capsule production, increased
102 sensitivity to bactericidal agents, including human complement, antibiotics, and other phages, and reduced
103 fitness in an *in vivo* bacteremia model. Here, we propose the use of phages, with *a posteriori* knowledge of their
104 receptors, to enable both effective antimicrobial treatment and the informed prediction of phage-resistance
105 outcomes, with exploitable fitness trade-offs extending the clinical impact of phage therapy.

106

Results

108 **Characterization of *Acinetobacter baumannii*-specific phages.** A group of nine *A. baumannii*
109 strains, from different sites of infection and exhibiting different antimicrobial resistance profiles were selected
110 for this study (31-35) (Fig. 1A). We used the Phage-on-Tap protocol (36) to isolate and purify phages into high-
111 titer preparations targeting the nine strains. Eight bacteriophages were isolated and used to establish an *A.*
112 *baumannii*-specific phage library. We tested the activity of the phages against all *A. baumannii* strains to
113 determine the host infectivity range (Fig. 1A). The phage with the broadest host range, øCO01, was capable of
114 productive infection in 4/10 strains, while phages øFG01, øCO02, øCO03 and øLK01 were highly specific and
115 capable of productive infection in only their host of isolation.

116 Phages øFG02 and øCO01 were chosen for further characterization based upon their contrasting host
117 ranges, high titers achievable during experimental amplification, and large phylogenetic distance between their
118 hosts of isolation (AB900 and the carbapenem-resistant isolate A9844, respectively). Plaque morphology of
119 both phages presented a distinctive hazy halo surrounding a zone of clear lysis (Fig. 1B). Microscopic
120 examination of the phages revealed virion lengths of ~250 nm for øFG02 and ~200 nm for øCO01, with
121 icosahedral capsids and sheathed contractile tails, consistent with the *Myoviridae* family of bacteriophages (Fig.
122 1C). The one-step killing curve of øFG02 demonstrated a latency period of approximately 40 min, with a burst
123 size of 15 plaque-forming units (PFU) per infection (Fig. 1D). For øCO01, the latency was ~41 min but the burst
124 size was doubled, at 30 PFU/infection (Fig. 1E).

A

Acinetobacter baumannii strain	Ref.	Site of infection	Phage Host Range							
			FG01	FG02	FG03	FG04	CO01	CO02	CO03	LK01
A9844	(33)	Unknown					*			
ATCC 19606	(35)	Urinary Tract								
AB5075	(34)	Osteomyelitis								
AB307-0294	(31)	Bloodstream								
AYP A22	(32)	Burn wound								
AB900	(31)	Perineal wound		*						
ATCC 17978	(31)	Spinal Meningitis								
APA2	(32)	Burn wound								
APA1	(32)	Wound swab								

0.008

Legend:
- Productive infection
- Non-productive infection
- No infection
- Host of Isolation
- * Phage-host pair analyzed in this study

B

øFG02 on AB900 — 1 cm

øCO01 on A9844 — 1 cm

C

øFG02 — 100 nm

øCO01 — 100 nm

D

One-step Killing Curve øFG02

Burst size = 15 PFU/cell

Latency ~ 40 min

$\emptyset$FG02 PFU/ml vs Time (min)

E

One-step Killing Curve øCO01

Burst size = 30 PFU/cell

Latency ~ 41 min

$\emptyset$CO01 PFU/ml vs Time (min)

F Genome of øFG02

75,277 bp

G Genome of øCO01

86,860 bp

Legend:
- DNA Replication
- Head protein
- Packing protein
- Capsid protein
- Hypothetical protein
- Tail fiber protein
- Integrase
- Neck protein
- Tail protein

H

OD_{600} vs Time (h)
- wt AB900
- wt AB900 + øFG02 (MOI = 1)
- wt AB900 + øFG02 (MOI = 0.1)
- LB Control

I

OD_{600} vs Time (h)
- wt A9844
- wt A9844 + øCO01 (MOI = 1)
- wt A9844 + øCO01 (MOI = 0.1)
- LB Control

125

4

126 **Figure 1.** Characterization of *Acinetobacter baumannii*-specific phages. A: Host range of the eight *A. baumannii*-specific
127 phages isolated in this study. Bacterial strains are ordered by the core-genome alignment phylogenetic tree on the left.
128 Productive infection is defined as lysis on a spot assay and production of plaques on a soft agar overlay, whereas non-
129 productive infection is defined as lysis on a spot assay with no plaques on a soft overlay agar. B: Plaque morphology of
130 phage øFG02 on host AB900 and øCO01 on host A9844, showing the central clearings or lysis zones surrounded by hazy
131 halos. C: Phage morphology as seen by transmission electron microscopy, øFG02 and øCO01 have icosahedral capsids
132 and contractile sheathed tails, characteristic of the *Myoviridae* family. D and E: One-step killing curves of phages øFG02
133 and øCO01 on their hosts of isolation. Latency time was measured from the beginning of the experiment to when the curve
134 at exponential growth reached the initial phage inoculum, whereas burst size was calculated by dividing the maximum free
135 phage count after bacterial burst by the initial phage titer in the experiment. Error bars represent standard error of the mean
136 (SEM) (n = 3). F and G: Genome assemblies of phages øFG02 and øCO01 show structural and replication genes for both.
137 The genome of øCO01 shows the presence of three predicted integrases. H and I: Growth curves of *A. baumannii* strains
138 AB900 and A9844 with and without phages. Phages were applied at two different multiplicities of infection (1 and 0.1). Lytic
139 activity of phages is shown by the drop in optical density shortly after initiation of the bacterial exponential growth phase;
140 and emergence of phage resistance is shown after 6 h of incubation. Each curve's top and bottom dotted lines show the
141 standard deviation (SD) (n = 3).

142

143 Genome sequencing of øFG02 generated a single contig of 75,277 bp (44.4% G+C), which best
144 matched with *Cronobacter* phage vB_CsaM_leN (90% coverage, 91.62% identity, GenBank accession number
145 KX431560.1). RAST annotation predicted 255 protein-coding regions, and the VIBRANT (37) analysis—which
146 uses multiple databases to annotate, determine the completeness and characterize virome function—revealed
147 that øFG02's genome possessed a lytic nature, and predicted several phage structural and replication genes
148 (Fig. 1F). For phage øCO01, we identified a contig of 86,860 bp (37.5% G+C) with a best match against
149 *Acinetobacter* phage Ab105-3phi (54% coverage and > 89% identity, GenBank accession number KT588073.1).
150 However, the contig also had high similarity (> 99% coverage and > 80% identity) with several *A. baumannii*
151 genomes from the NCBI database and the VIBRANT analysis was negative for a lytic feature. Annotation of the
152 contig revealed integrase genes along with phage structural genes (Fig. 1G). Based on this finding, we
153 attempted to experimentally produce A9844 lysogens containing øCO01 via coincubation. We performed the
154 experiment with two different concentrations of øCO01, and screened 18 colonies from each, without success
155 (Fig. S1). This suggests that despite the presence of a predicted integrase in the genome of øCO01, it is
156 incapable of lysogenizing its host of isolation, at least under regular *in vitro* conditions.

157 To further demonstrate the lytic activity of the phages, we coincubated them with their bacterial hosts
158 at two different multiplicities of infection (MOI), 1 and 0.1. The growth curves (Fig. 1H and 1I) show phage lytic
159 activity beginning during the bacterial exponential growth phase, with the bactericidal effect occurring earlier at
160 a higher MOI. Both phages inhibited bacterial growth for just over 6 h and shortly thereafter, regardless of the
161 phage MOI used, the strains developed phage-resistance and resumed growth *in vitro*.

162 **Isolation of phage-resistant *A. baumannii* mutants.** Bacteria are known to quickly develop phage-
163 resistance when subjected to the selective pressure of lytic phages *in vitro*. We coincubated strains AB900 and
164 A9844 in a semi-solid culture with phages øFG02 and øCO01, respectively. Colonies that were able to grow in
165 the center of lysis zones (Fig. S2) subsequently underwent two single-colony isolation steps. Next, we
166 performed inverted spotting assays (Fig. 2A and 2B) and growth curves (Fig. 2C and 2D) to confirm the phage-
167 resistant phenotype of the selected colonies. From these assays, we picked a single mutant of strain AB900
168 that was resistant (R) to phage øFG02 (øFG02-R AB900) and a single mutant of strain A9844 that was resistant
169 (R) to phage øCO01 (øCO01-R A9844). *In vitro,* phage-resistant mutants did not revert to the wild type

170 phenotype despite ≥ 10 growth cycles (defined as the subculture on a liquid or solid medium without the

171 presence of phage). Growth curves showed a 3% increase in area under the curve (AUC) for øFG02-R AB900

172 and a 9% decrease for øCO01-R A9844 when compared to their wild type counterparts (Fig. S3).

173
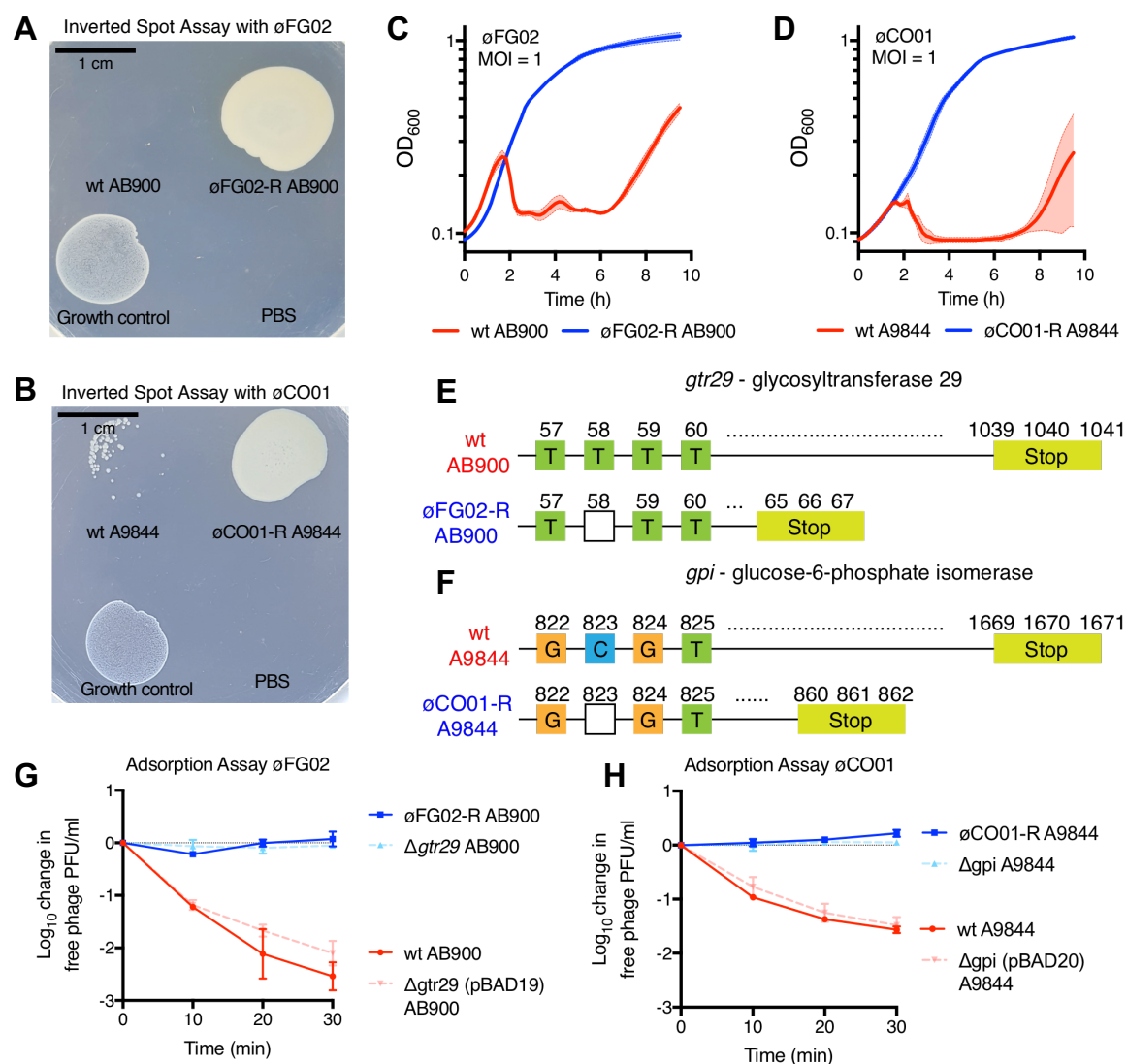
174
175

176 **Figure 2.** *A. baumannii* phage-resistant mutant strains, phage receptors and mechanism of phage resistance. A and B:

177 Inverted spot plate assay containing 10^8 PFU of phages øFG02 or øCO01. Lack of confluent growth of AB900 and A9844,

178 and confluent growth of øFG02-R AB900 and øCO01-R A9844 suggest phage-resistant phenotype. PBS used as a negative

179 control, and *Enterococcus faecium* as a bacterial growth control. C and D: Growth curves in the presence of phages at an

180 MOI of 1. Wild type strains AB900 and A9844 (in red) were affected by phage activity, whereas phage resistant mutants

181 øFG02-R AB900 and øCO01-R A9844 (in blue) grew unaffected. Shaded zones represent SD (n = 3). E and F: Mutations

182 identified in øFG02-R AB900 and øCO01-R A9844 associated with the phage-resistant phenotype. For both strains, the

183 affected genes are in the K locus, and the single-nucleotide deletions led to premature truncation of the proteins. G and H:

184 Phage adsorption assay, $\log_{10}$ reduction in free phage titers over a 30 min interval after mixing phages and hosts. Each

185 phage was mixed with either wild type, phage-resistant, knockout mutant, or plasmid-complemented hosts. Phages adsorb

186 to phage-sensitive strains (wild type and plasmid-complemented, shades of red) leading to a decrease in free phage titer,

187 whereas phages do not adsorb to phage-resistant strains (phage-resistant, knockout mutant, shades of blue). Error bars

188 represent SEM (n = 3).

189

6

Identification of phage receptors and phage-resistance mechanisms in *A. baumannii*. With the purpose of identifying the number, type, and loci of the mutations granting phage-resistance to our *A. baumannii* strains, we extracted genomic DNA from the wild type strains AB900, A9844 and their phage-resistant counterparts øFG02-R AB900 and øCO01-R A9844. Illumina® HiSeq 150 bp paired-end reads were used for a pairwise comparison of the bacterial genomes. In each phage-resistant strain, a single nucleotide deletion in a gene within the K locus was found (Fig. 2E and 2F). Genes in the K locus of *A. baumannii* regulate the production, modification and export of capsular polysaccharides (38). For øFG02-R AB900, the affected gene was *gtr29*, which codes for a glycosyltransferase and in øCO01-R A9844 it was *gpi,* which codes for the enzyme glucose-6-phosphate isomerase. In both cases, the identified deletions caused codon frameshifts resulting in the premature truncation of the proteins, at amino acid 21 out of 346, and 286 out of 556 for the glycosyltransferase and glucose-6-phosphate isomerase, respectively (Fig. 2E and 2F).

To demonstrate that the identified mutations were responsible for the phage-resistant phenotypes, we disrupted genes *gtr29* and *gpi* in AB900 and A9844, respectively, using a kanamycin-resistance cassette. Next, we used the newly-obtained strains Δgtr29 AB900 and Δgpi A9844 in an efficiency of plating (EOP) assay and confirmed they were completely resistant to phages øFG02 and øCO01, respectively (EOP = 0%). Complementation analysis showed restoration of phage susceptibility (EOP = 100%), thus confirming the involvement of genes *gtr29* and *gpi* in phage infectivity.

Both *gtr29* and *gpi* are in the K locus and thus predicted to function in biosynthesis of capsular polysaccharides. We hypothesized that phages øFG02 and øCO01 used capsular polysaccharides as their receptors, and that the loss or modification of such receptors led to lack of phage adsorption and subsequent phage-resistance in *A. baumannii*. To test the hypothesis, we performed an adsorption assay using each phage and their respective strain set (wild type, phage-resistant isolate, knockout mutant and plasmid-complemented mutant) (Fig. 2G and 2H). Within 30 min, more than 99% and 97% of øFG02 and øCO01 particles had adsorbed to their respective wild type hosts. In contrast, the titers of free phage particles did not decrease when the phages were mixed with either the phage-resistant or knockout mutants, demonstrating the inability of phages to adsorb to these bacterial cells. As expected, phage adsorption was reinstated in the plasmid-complemented strains expressing *gtr29* and *gpi.* The adsorption assay supported our hypothesis that capsular polysaccharides are the phage receptor for øFG02 and øCO01 and that phage-resistance arose through alteration or loss of these receptors leading to inhibition of phage adsorption.

***A. baumannii* phage-resistant strains exhibit phenotypic trade-offs.** As a next step, we sought to investigate if our phage-resistant *A. baumannii* strains would exhibit detrimental phenotypic trade-offs associated with their acquired mechanism of phage-resistance. We began tackling this question by assessing the production of capsular polysaccharides in the phage-resistant strains.

First, we used Maneval's staining technique to visually evaluate capsule production (Fig. 3A). Capsules were observed as unstained halos surrounding each bacterial cell (stained in pink), and the thickness of such halos is a proxy of capsule production. Wild type strains AB900 and A9844 were uniformly capsulated, whereas most of the cells of øFG02-R AB900 and øCO01-R A9844 appeared to lack capsules. Single cell imaging using scanning electron microscopy (SEM) (~100 cells per strain observed, consistent phenotypes throughout the observations), suggested that the surface of wild type A9844 possessed a complex polysaccharide capsule, including many pilus-shaped protrusions. In contrast, the appearance of the phage-resistant surface suggested loss of capsule. Less obvious differences were noted between AB900 and øFG02-R AB900 (Fig. 3B and S4). For a quantitative assessment of the phenotype, we assayed the production of surface polysaccharides using

7

232 the colorimetric sulfuric acid and phenol assay (39) (Fig. 3C). Using this technique, we observed 2.2-fold and

233 3-fold decrease in polysaccharide production in øFG02-R AB900 and øCO01-R A9844, respectively, compared

234 to their wild type strains (n = 3; 79 ± 1.7 µg/ml vs. 35.6 ± 8.8 µg/ml [mean ± SD]; unpaired t test; p = 0.001; two-

235 tailed; for AB900 vs. øFG02-R AB900) (n = 3; 179.9 ± 15.6 µg/ml vs. 58.1 ± 5.6 µg/ml; unpaired t test; p =

236 0.0002; two-tailed; for A9844 vs. øCO01-R A9844). In accordance, colonies of strains AB900 and A9844

237 exhibited a mucoid phenotype—viscous and sticky colonies—characteristic of capsule production, which was

238 lost in colonies of øCO01-R A9844 but not in øFG02-R AB900. Taken together, our findings indicate a major

239 defect in the overall production of capsule polysaccharides in the phage-resistant mutant strains, with these

240 results being consistently more pronounced in øCO01-R A9844.

241 　　　　Capsular polysaccharides aid in the attachment of bacterial cells to biotic and abiotic surfaces, which is

242 the first step in the formation of biofilms (16), one of the hallmarks of *A. baumannii* clinical infections. Having

243 observed a significant decrease in capsule production in the phage-resistant mutants, we tested if these mutants

244 had impaired biofilm production. We compared the ability of the strains to form biofilms on a polystyrene surface

245 at 48 h (Fig. 3D). As expected, the phage-resistant strains øFG02-R AB900 and øCO01-R A9844 had a 2.1-

246 fold and 3.6-fold reduction, respectively, in biofilm production when compared to their wild type counterparts

247 (Fig. 3E) (n = 3; optical density of biofilm 1 ± 0.1 vs. 0.5 ± 0.1 [mean ± SD]; unpaired t test; p = 0.0038, two-

248 tailed; for AB900 vs. øFG02-R AB900) (n = 3; 1.3 ± 0.2 vs. 0.4 ± 0.03; unpaired t test; p = 0.001, two-tailed; for

249 A9844 vs. øCO01-R A9844). Thus, the acquisition of phage-resistance in our *A. baumannii* strains resulted in

250 the phenotypic trade-offs of impaired capsule production and biofilm formation.

251
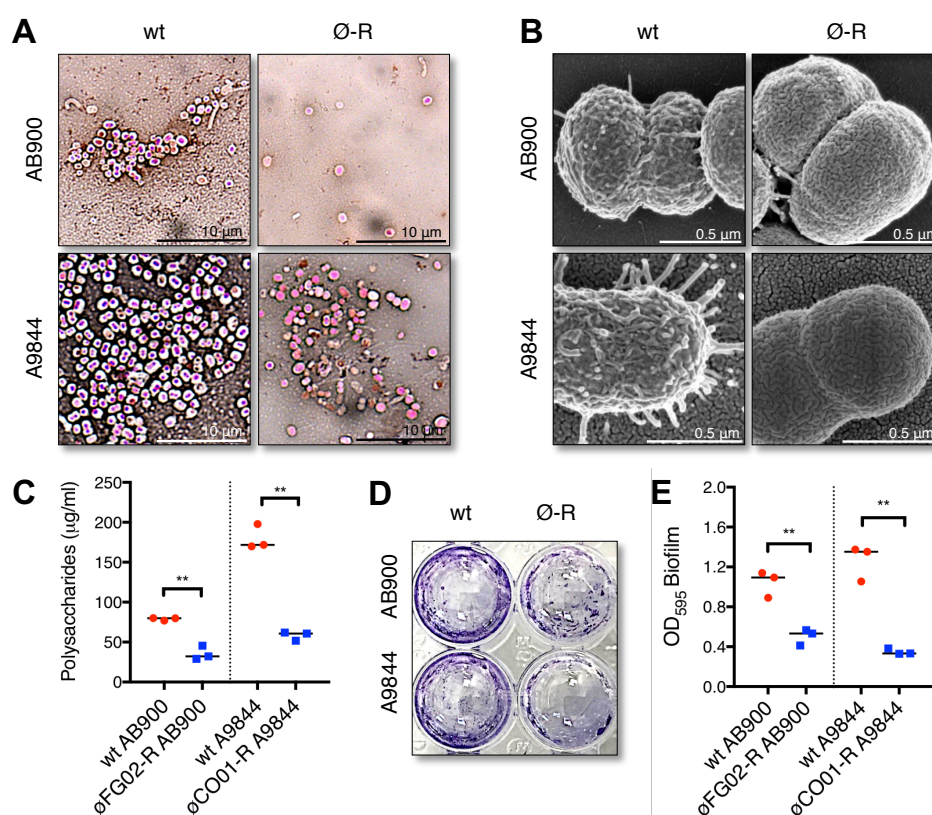
252

253 **Figure 3.** Phenotypic trade-offs of phage-resistance in *A. baumannii.* A: Microscopic inspection of capsule thickness in

254 slides stained using the Maneval's technique. B: Cell surface appearance as observed via scanning electron microscopy,

255 representative images from ~100 observations (additional images in Fig. S4). C: Production of capsule polysaccharides

256 measured by absorbance of a colorimetric phenol-sulfuric acid reaction and extrapolated to a standard curve (Fig. S5). D

257 and E: Biofilm production on a polystyrene surface at 48 h, measured by absorbance of crystal-violet stained and ethanol-

258 solubilized biofilm. For the scatterplots in panels C and E, wild type strains represented in red and phage-resistant mutants

259 in blue, bars represent medians (n = 3), each point represents the average from three technical replicates, unpaired t test **

260 = p < 0.005, two-tailed.

261

262 **Phage-resistant *A. baumannii* strains are more susceptible to antimicrobial agents.** Capsules and

263 biofilms are major virulence determinants in *A. baumannii.* Part of their importance in bacterial pathogenesis

264 relies on enabling *A. baumannii* to evade components of the host's immune response and to resist the effect of

265 several antibiotics. Following the observed trade-offs of our *A. baumannii* phage-resistant mutants, we

266 hypothesized the mutants would have become vulnerable to the action of various antimicrobial agents.

267 The complement system consists of a cascade of serum proteins capable of eliminating pathogens by

268 attacking their membrane, and enhancing the activity of antibodies and phagocytes. We established a serum

269 killing assay to determine the susceptibility of *A. baumannii* to the action of the human complement system (Fig.

270 4A). Over a period of 180 min, wild type strains AB900 and A9844 withstood the effect of, and even grew in,

271 human serum. Conversely, the phage-resistant mutants øFG02-R AB900 and øCO01-R A9844 were reduced

272 below the level of detection in the serum even at the first timepoint of 45 min, representing a >4-log decrease.

273 The results shown in the experiment can be safely attributed to the action of the complement system, as the

274 antimicrobial effect was lost if heat-inactivated serum was instead used (data not shown).

275 As our mutants demonstrated heightened sensitivity to complement, we next sought to determine

276 whether their susceptibility to seven clinically relevant antibiotics was also impacted. We used the microbroth

277 dilution method and the CLSI guidelines for clinical interpretation (Fig. 4B, raw data in Table S1). Although

278 AB900 is not an MDR strain, it is resistant to ceftazidime, a third-generation cephalosporin. The phage-resistant

279 mutant strain øFG02-R AB900 presented a 16x decrease in the minimum inhibitory concentration (MIC) of

280 ceftazidime, becoming sensitive to it, as well as 2x decrease in the MIC of fellow beta-lactams ampicillin +

281 sulbactam and imipenem, and the fluoroquinolone ciprofloxacin. In contrast, A9844 is an MDR, carbapenem-

282 resistant isolate, considered by the CDC as a priority pathogen. We observed that øCO01-R A9844 presented

283 a 2x reduction in the MIC of minocycline and ampicillin + sulbactam. The latter resulted in a change of the

284 clinical interpretation of the MIC, making A9844 sensitive to ampicillin + sulbactam. However, øCO01-R A9844

285 also exhibited a 2x increase in the MIC for the aminoglycoside amikacin, but without a change in the clinical

286 interpretation. The findings show instances of antibiotic resensitization occurring as a trade-off of phage-

287 resistance in *A. baumannii.*

288 Finally, we tested another antimicrobial strategy, our *A. baumannii*-specific phage library, against

289 strains øFG02-R AB900 and øCO01-R A9844 for extended phage-host range (Fig. 4C). We observed that,

290 upon acquiring resistance to phage øFG02, strain øFG02-R AB900 became sensitive to phage øLK01, which

291 was previously only capable of non-productive infection in wild type AB900. Furthermore, strain øCO01-R

292 A9844 became vulnerable to the lytic action of three new phages, øFG01, øFG02 and øLK01. In summary,

293 acquisition of phage-resistance was accompanied by resensitization to at least three different types of

294 antimicrobial agents. This discovery is relevant, as all of the agents can play a role in the clinical setting during

295 the treatment of *A. baumannii* infections.

296
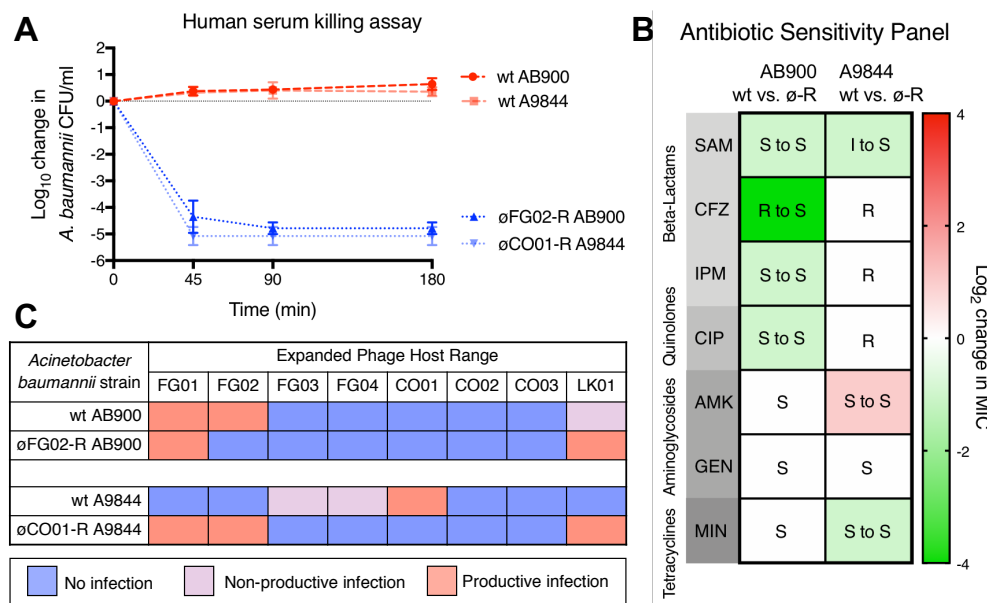
Figure 4. Increased sensitivity of phage-resistant *A. baumannii* to antimicrobial agents. A: Human serum killing assay. Freshly-thawed human serum was inoculated with 10^5 CFU/ml of *A. baumannii,* and the change in bacterial load was measured at regular intervals. Wild type strains (shades of red) grew in serum whereas phage-resistant strains (shades of blue) were rapidly killed; error bars represent SEM (n = 3). B: Antibiotic sensitivity pattern. The minimum inhibitory concentrations (MICs) of 7 antibiotics, from 4 pharmacological groups were measured using the microbroth dilution method. The median (n = 3) of the $\log_2$ change in MIC between the wild type and phage-resistant strains is color coded, with shades of green showing a reduction in MIC in phage-resistant mutants, shades of red showing an increase in MIC, and white showing no change for each specific antibiotic. Inside each cell, the clinical interpretation of the MIC is shown (S = Sensitive, I = Intermediate, R = Resistant). Raw data values are available in Table S1. SAM: ampicillin + sulbactam, CFZ: ceftazidime, IPM: imipenem, CIP: ciprofloxacin, AMK: amikacin, GEN: gentamicin, MIN: minocycline. C: Expanded phage host range map of the *A. baumannii*-specific phage library against øFG02-R AB900 and øCO01-R A9844 reveals sensitization to additional phages.

Phage-resistant *A. baumannii* strains show decreased fitness *in vivo*. The trade-offs of impaired capsule production and resensitization to antimicrobials could affect *A. baumannii*'s ability to invade and survive in mammalian hosts (40, 41). We therefore sought to observe the *in vivo* fitness of our phage-resistant mutants. To achieve this, we established a murine model of septicemia via intraperitoneal injection of 10^6 CFU with 6% porcine stomach mucin. Groups of 6-to-10 weeks old, female, BALB/c mice (n = 4) were infected with either AB900, A9844, or their phage-resistant counterparts. After 8 h, the levels of bacterial colonization were assessed for the blood, liver, kidney and spleen. In both strain pairs, we observed a 2-log reduction of bacterial load in solid organs and a >3-log reduction in blood for phage-resistant mutants, when compared to wild type strains (Fig. 5A and 5B) (n = 4; Mann-Whitney test, p = 0.0286 for all comparisons except kidney in A9844 [p = 0.0571], two-tailed). Interestingly, after their passage through the animal hosts, øCO01-R A9844 bacteria did not revert to the wild type form, but in 2 out of the 4 mice infected with øFG02-R AB900 there was evidence of reversion to wild type AB900. This reversion was only seen in bacteria retrieved from solid organs and not blood and, in one of the animal hosts, it was heterogeneous, meaning that populations of both wild type-reverted and phage-resistant mutants were retrieved. These observations supported the hypothesis that phage-resistant *A. baumannii* suffers a fitness cost *in vivo*.

10
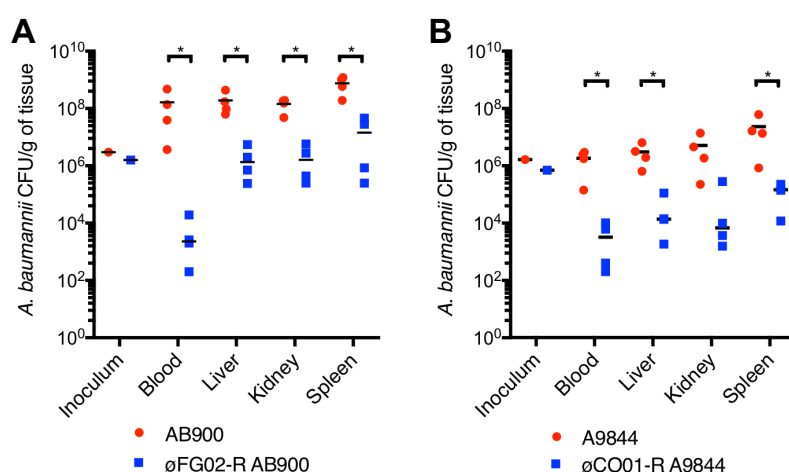
Figure 5. *In vivo* fitness is reduced in phage-resistant *A. baumannii.* 4 groups of 4 female, 6-to-10 weeks old, BALB/c mice were subjected to intraperitoneal (IP) injection of 10^6 colony forming units of either AB900, A9844, øFG02-R AB900 or øCO01-R A9844. At the humane endpoint of 8 h, blood, liver, kidney and spleen were collected for bacterial quantification. A and B: Bacterial burdens at 8 h post infection, normalized by tissue weight. Wild type strains in red, phage-resistant strains in blue. Each data point represents an animal, with black bars representing the median values, Mann-Whitney test * = p < 0.05, two-tailed.

Discussion

Antibiotic-resistant *A. baumannii* was recently deemed the top priority pathogen requiring new therapeutic strategies (4), and it certainly is one of the most threatening pathogens encountered in clinical practice (8). In this study, we isolated novel phages against a phylogenetically diverse panel of *A. baumannii* strains and provided a detailed characterization of two of them: øFG02 and øCO01. Despite the strong lytic activity of these phages, we observed the rapid emergence of phage-resistant mutants *in vitro*. Phage-resistance is often seen as a prominent road-block for efficacious phage therapy, with up to 80% of preclinical and clinical phage therapy trials reporting emergence of phage-resistant mutants (42). Detailed characterization of phage biology and identification of host receptors enabled us to identify the mechanism of phage-resistance in this pathogen. Phage-resistant strains harbored loss-of-function mutations in genes of the K locus, which are responsible for the biosynthesis of capsular polysaccharides. Using genetic engineering, we confirmed that disruption of glycosyltransferase 29 and glucose-6-phosphate isomerase led to phage-resistance in *A. baumannii* strains AB900 and A9844, respectively. Furthermore, an adsorption assay supported our hypothesis that phage-resistance emerged through disruption the phage receptors resulting in lack of phage adsorption. We also determined that capsule loss in phage-resistant *A. baumannii* is associated with a reduction in biofilm formation, resensitization to antimicrobial agents including antibiotics, human complement, and additional phages, and a reduction in fitness in a murine model of bacteremia. These results demonstrate that the capsular polysaccharides of *A. baumannii* are the receptors for phages øFG02 and øCO01. To the best of our knowledge, this is the first confirmation of a phage receptor in this key MDR superbug. These findings provide a step towards the exploitation of the fitness trade-offs of phage-resistance and improvement in the clinical translation of phage therapy.

The therapeutic use of lysogenic phages is subject to ongoing debate. Their use is normally inadvisable due to risks such as lysogenic conversion of the host, or reduced clinical effect (17). However, in the absence of lytic phages against a particular pathogen, or in emergency cases, their use might be justified (17). The

genomic analysis of one of our phages, øCO01, revealed three putative integrase genes and significant sequence homology with *A. baumannii* genomes, suggesting a possible lysogenic nature. Although we cannot conclusively rule out the possibility of temperate behavior in øCO01, the phage displayed strong lytic activity in phenotypic assays (Figs. 1B, 1E and 1I), and was not able to lysogenize its host of isolation, A9844, *in vitro* (Fig. S1). Notably, the sequence analysis of øCO01 revealed a best match to *Acinetobacter* phage Ab105-3phi with a modest 54% coverage and >89% identity, so further investigation of gene function in øCO01 is warranted. It is possible that øCO01 emerged through recombination between a lytic and a lysogenic phage, and while it contains putative integrases, it behaves as a lytic phage on host A9844 under *in vitro* conditions. We suggest that experimental validation of a phage's capacity to lysogenize a host, rather than simply the presence of a putative integrase gene, may be a more appropriate determinant for the selection of phages for therapeutic use.

Bacterial capsules have been demonstrated to be key virulence factors (11, 16). In *A. baumannii,* capsule biosynthesis is a complex and well-regulated process that involves up to 10 different groups of proteins (16, 38). The capsule is comprised of tightly packed repeating subunits (K units) that consist of 4 to 6 sugars, with a large diversity of K unit structures identified to date (16, 23). From our phage-resistant *A. baumannii* isolates, we identified mutations in two enzymes that are required for the early stages of K unit production. Specifically, the enzyme glucose-6-phosphate isomerase catalyzes the conversion of glucose-6-phosphate to fructose-6-phosphate, forming one of the many simple sugars that can constitute part of a K unit, while the glycosyltransferase is required to assemble specific sugars into the growing chain of the K unit. The biochemical structures of the K units of the capsules of AB900 and A9844 have been previously described (23, 43, 44). However, the exact effects that our mutations had on these structures were not elucidated here and were outside the scope of this study. As a result, we were only able to conclude that phages øFG02 and øCO01 use the capsule polysaccharides of *A. baumannii* as receptors, a phenomenon previously described for phages targeting the pathogens *Campylobacter jejuni* (45), *Salmonella enterica* (46) and *Klebsiella pneumoniae* (47), with the specific K unit polysaccharide structure remaining to be identified.

The most clinically important trade-off of phage-resistance observed in our *A. baumannii* strains was perhaps the resensitization to three types of antimicrobial agents. Antibiotic resensitization could be broadly explained through loss of capsule, theoretically making it easier for the drugs to access their target site. However, the fact that resensitization primarily occurred towards beta-lactams—which act via disruption of the cell wall—suggests a more specific mechanism. It has been described, for example, that inactivating mutations in genes encoding the Wzc or Wza components of the capsule secretion system in *A. baumannii* also lead to increased susceptibility to beta-lactams (11). It is possible that capsule-deficient bacterial cells have a lower tolerance threshold to further disruptions in components of the cell envelope. Further research is needed to determine if antibiotic protection provided by *A. baumannii* capsules is strain specific, capsule-type specific, or universal (16). It is also worth noting that despite the microbroth dilution method being the gold standard for antibiotic sensitivity testing (48), we cannot rule out the influence of test variability in our results, particularly in changes in MIC ≤ 2x between wild type and phage-resistant mutants. Susceptibility to complement-mediated killing can also be explained by the loss of capsule, as the hydrophilicity and negative charge of capsule sugars would normally limit complement deposition on the bacterial surface (11). Finally, the alteration of the surface polysaccharides in the phage-resistant mutants could have unmasked or generated other receptors that were recognized by additional phages, explaining the observed changes in the phage host range, and allowing us to enhance and extend the use of phage therapy. Interestingly, both phages analyzed in this study presented plaque morphologies of lytic centers surrounded by hazy halos (Fig. 1B), which suggest the production of

401 depolymerases, enzymes capable of digesting capsular polysaccharides (49). Further research could pursue

402 the purification and characterization of the biological activity of these enzymes, attempting to replicate the

403 described effects of capsule loss in *A. baumannii.*

404 Despite being situated within the K locus in *A. baumannii,* the physiological role of glycosyltransferase

405 29 and glucose-6-phosphate isomerase may go beyond capsule production. Genes from the K locus are also

406 used during the biosynthesis of outer membrane lipooligosaccharides (16), and some of the proteins they

407 encode have been described as "multitaskers" involved in bacterial virulence and metabolism (50). As such, it

408 is possible that further effects of the disruption of *gtr29* and *gpi,* unrelated to capsule loss, could be identified in

409 our phage-resistant mutants. Altered production of glycosyltransferases and glucose-6-phosphate isomerase

410 has been previously shown to affect virulence and resistance to antimicrobials through different routes in a few

411 pathogens. Boinett et al. (51) identified *gpi* and at least two glycosyltransferases as some of many upregulated

412 genes in colistin-resistant strains of *A. baumannii.* Zhang et al. (52) demonstrated that isomerase-deficient

413 mutants of the fungal pathogen *Cryptococcus neoformans* had reduced capsule biosynthesis, disruptions in

414 their cell wall and plasma membrane and exhibited hypersensitivity to osmotic stress. Moreover, Tsuge et al.

415 (53) noted a significant reduction in virulence upon inactivation of glucose-6-phosphate isomerase in the plant

416 pathogen *Xanthomonas oryzae,* possibly due to impaired carbohydrate uptake. Investigating further trade-offs

417 in our phage-resistant mutants could lead to the discovery of other clinically exploitable phenotypes.

418 Our results suggest that the capsule of *A. baumannii* acts as a phage receptor and tropism determinant.

419 We worked with two *A. baumannii* phages isolated from phylogenetically distant strains, both of which induced

420 loss-of-function mutations: although distinct, the affected genes were located within the same locus and are

421 both involved in the production of capsular polysaccharides. This is further supported by recent studies

422 documenting that phage tail fibers directly interact with *A. baumannii* capsular polysaccharides (54, 55) and a

423 phage therapy case study treating a complicated MDR *A. baumannii* infection that reported capsule loss upon

424 emergence of phage-resistance (22). However, it should be noted that all these studies have focused on a small

425 number of phages and that other *A. baumannii* phage receptors are likely.

426 We attribute the emergence of phage-resistance to the loss of *A. baumannii*'s capsule, which

427 subsequently results in clinically exploitable fitness trade-offs. However, our study has only characterized a

428 single phage-resistant isolate, each, from AB900 and A9844, and there exists the potential for other

429 independently evolved resistance mutations to emerge that lack these phenotypes. Thus, a key question is

430 whether the evolution of phage-resistance in *A. baumannii* is repeatable and predictable. An analysis of the K

431 loci in heterogeneous populations of phage-resistant mutants could demonstrate the diversity of mutations

432 occurring therein or, conversely, point to other pathways of phage-resistance evolution not involving the K locus.

433 Finally, an important follow-up experiment should aim to identify whether the mechanisms of phage-resistance

434 acquisition reported here also occur *in vivo.*

435 We previously theorized an approach to phage therapy delivery based on the exploitation of phage-

436 resistance (17). As demonstrated in this study, the emergence of phage-resistance in *A. baumannii* can be

437 accompanied by exploitable trade-offs. But in order to consistently and reliably take advantage of them, we

438 require a detailed characterization of the phages, their hosts, their receptors and their mechanisms of infection

439 and resistance. Ideally, this approach to phage therapy would employ phages that exhibit strong antimicrobial

440 effects, and force a predictable evolutionary response by the pathogen, through known mechanisms of phage-

441 resistance, thereby allowing physicians to foresee their next therapeutic intervention and stay a step ahead of

442 the pathogen (Fig. 6). In a previous clinical case of phage therapy use against MDR *A. baumannii* (22), where

443 the trade-offs of capsule loss and resensitization to an antibiotic were seen in phage-resistant mutants, these

444 findings were not anticipated nor mechanistically explained, arguably limiting their efficient clinical exploitation.

445   The ultimate goal of our research is to enable the successful clinical translation of phage therapy against

446 *A. baumannii* and other MDR pathogens. Importantly, the findings of our study highlight that phage therapy

447 should not be proposed as a replacement for antibiotic therapy. In fact, we demonstrate that phages can be

448 used not only for their lytic activity, but, when combined with *a posteriori* knowledge of receptors and emergence

449 of phage-resistance, as a resensitization strategy empowering other antimicrobial agents. Improving the

450 efficacy, and furthering the clinical impact of phage therapy, is an important step in the fight against the

451 postantibiotic era.

452
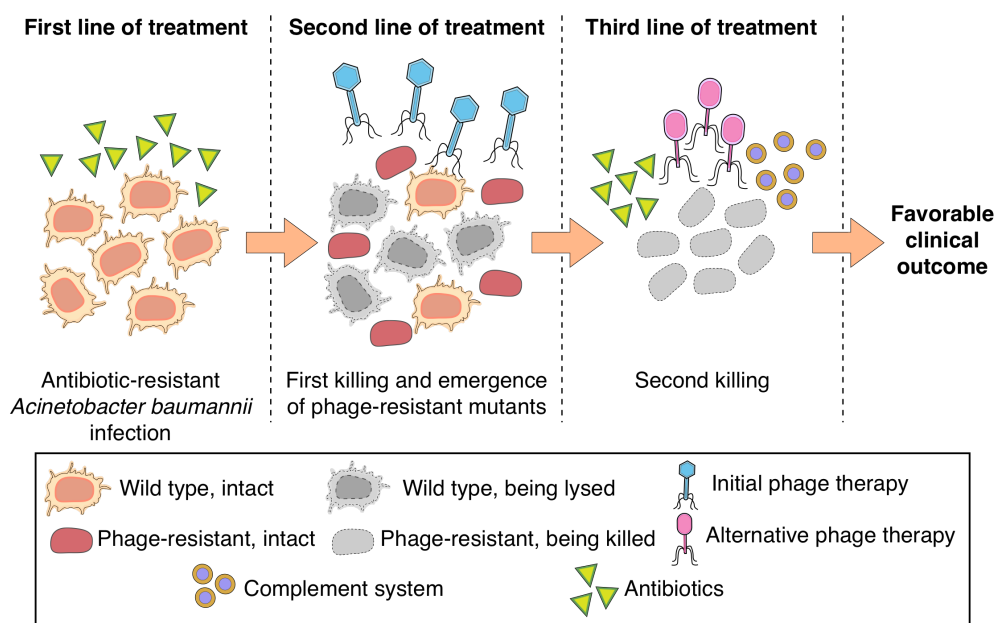
453

454 **Figure 6.** An approach toward phage therapy utilizing lytic activity of phages, *a posteriori* knowledge of receptors, predictable

455 emergence of phage-resistance and exploitation of fitness trade-offs. An MDR *A. baumannii* infection (capsulated red cells)

456 will typically withstand antibiotic treatment (first line of treatment). We can pursue the use of phage therapy (second line of

457 treatment), the lytic activity of the phages resulting in a first killing and the emergence of phage-resistant mutants

458 (unencapsulated red cells). We can exploit the trade-offs of phage-resistance using a third line of treatment that can include

459 re-potentiated antibiotics, alternative phages, and the immune system. This will result in a second killing leading to an

460 improved clinical outcome.

461

Materials and Methods

463   **Bacterial strains, plasmids, and culture conditions.** A complete list of strains and plasmids used in

464 this study can be found in Table S2. Bacteria were cultured using either lysogeny broth (LB) or Mueller Hinton

465 broth (MHB) (Sigma-Aldrich, Australia), at 37 °C with aeration, supplemented with agar and/or 50 μg/ml of

466 kanamycin sulfate, as required.

467   **Phage isolation, amplification and storage.** Phages were isolated from raw sewage samples

468 obtained from several states in Australia (Queensland, New South Wales, and Victoria). Aliquots of sewage

469 were combined with overnight cultures of up to three bacterial strains, and supplemented with 10x LB and 10

470 mM CaCl$_2$ and MgSO$_4$. Mixtures were incubated overnight and the resulting lysates were purified with the

471 previously described Phage-on-Tap protocol (36). The lysates were titrated in plaque forming units (PFU) per

472 ml and stored at 4 °C.

473 **Determination of phage host range and efficiency of plating.** The lytic activity of each phage was

474 screened against nine *A. baumannii* strains with the standard spot assay as previously described (56). For

475 comparing the efficiency of phage infection between hosts, the efficiency of plating (EOP) assay was used.

476 Overnight bacterial cultures were standardized to an optical density at 600 nm (OD$_{600}$) of 0.3 using a

477 spectrophotometer. This density was previously assessed to be roughly equivalent to 5×10^7 CFU/ml. Next, soft

478 agar overlays were set up with known concentrations of phage lysate (10^1-10^3 PFUs). After incubation, the

479 plates were inspected for plaques and the average number of plaques was recorded and compared as a

480 percentage of the plaques found in the original host of isolation.

481 **Transmission Electron Microscopy (TEM).** Further purification of the phage lysates, using the

482 Vivaspin 6 centrifugal concentrator (MWCO 1,000,000 kDa) (Sartorius, Australia), was required for high-quality

483 electron microscopy visualization. Then, 10 μl droplets of phage suspension were placed on copper TEM grids

484 (200 mesh, SPI, USA) with carbon-coated ultrathin (invisible on the water surface) formvar film (57). They were

485 left for 30 seconds and then dried using filter paper. A 10 μl droplet of uranyl acetate water solution (1% w/v)

486 was then added to the grid surface and left for 20 seconds. The grid was dried with filter paper, and then

487 examined under a TEM (JEM-1400 Plus; Jeol, Japan) at an accelerating voltage of 80 kV.

488 **One-step phage killing curves and adsorption assay.** Bacteria from overnight cultures and phages

489 from pure lysates were mixed at a multiplicity of infection (MOI) of 0.01 (10^6 PFU/ml to 10^8 colony forming units

490 [CFU]/ml) in LB. The suspensions were incubated at 37 °C with aeration. At each timepoint, samples of the

491 suspensions were transferred into chloroform-saturated PBS, vortexed, and then centrifuged at 3,500x g for 3

492 min. The supernatant was diluted in PBS and plated in duplicate for quantification of free phage particles.

493 **Extraction of phage DNA, minION sequencing and phage genome analysis.** A starting volume of

494 1.8 ml of phage lysate with a concentration of > 10^{10} PFU/ml was treated with DNase and RNase A. DNA was

495 extracted using the phenol-chloroform method and purified with isopropanol and sodium acetate as described

496 previously (58). The extracted DNA was dissolved in nuclease free water, then quantified and its purity assessed

497 using a Nanodrop (NanoDrop Technologies, Wilmington, DE, USA), Qubit fluorometer (Life Technologies,

498 Carlsbad, CA, USA), and 1% agarose gel electrophoresis. 1 μg of DNA was used for library preparation using

499 the Ligation Sequencing Kit 1D (SQK-LSK109, Oxford Nanopore Technologies, ONT, Oxford UK) following the

500 manufacturer's instructions. The sequencing libraries were multiplexed and loaded into the Flow Cell FLO-

501 MIN106 Spot-ON of the MinION system using a Library Loading Bead Kit R9 according to the manufacturer's

502 instructions. The raw reads were obtained using MinKNOW v1.7.14 in a 48 h-run experiment and base calling

503 was performed using ONT default software. Deepbinner v0.2.0 (59) was used to demultiplex the raw reads.

504 Reads smaller than 500 bp were removed using Trimmomatic v.039 (60) and the remainder assembled using

505 Unicycler v0.4.3 (61). Genome annotation was performed by combining multiple tools: the RAST server (62),

506 PHASTER (63) and VIBRANT (37).

507 **Lysogen isolation.** Based on a previously described protocol (64), a spot assay was established with

508 the phage-host pair of interest. After 48 h of incubation, cloudy and confluent centers of bacterial growth within

509 zones of lysis were identified. Bacterial growth from these zones was scraped off using a sterile loop and streak-

510 plated. After overnight incubation, 36 colonies were tested for lysogeny using a patch test. For this test, single

511 colonies were patch-plated onto two LB plates, the second one of which contained a soft agar lawn of the wild

512 type host. After 48 h of incubation, the plates were examined looking for halos of lysis around the patches of

513 the second plate. All presumptive lysogens then underwent three rounds of single-colony purification before

514 repeating a patch test. Finally, liquid cultures of the possible lysogens were pelleted, and the supernatants were

515 filtered through a 0.2 μm filter and tested for spontaneous phage release using spot assays.

516 **Bacterial kinetics.** Growth kinetics were determined using a 96 well plate format, measuring OD_{600}

517 every 10 min with a starting inoculum of 10^6 CFUs, unless otherwise specified, and phage PFUs at MOIs of

518 either 0, 1 or 0.1. Where required, area under the curve (AUC) was calculated from a baseline of y = 0.1 and

519 the percent difference calculated (65).

520 **Isolation of phage-resistant *A. baumannii* mutants.** Following the same principle as the spot assay,

521 25 μl aliquots of pure lysate (concentration > 10^8 PFU/ml) were spotted onto bacterial lawns. After an overnight

522 incubation, bacterial colonies growing in the middle of lysis zones were picked and streaked onto LB agar plates

523 for two rounds of single-colony isolation. The phage-resistant phenotypes were confirmed using three methods:

524 inverted spot plate assays (66), standard soft agar overlay assays, and *in vitro* growth curves. Phage-resistant

525 mutant strains were tested bimonthly to ensure reversion to a phage-sensitive phenotype did not occur.

526 **Extraction of bacterial genomic DNA, sequencing, bacterial genome comparison and**

527 **phylogenetic analysis.** The GenElute™ Bacterial Genomic DNA Kit protocol (Sigma-Aldrich, Australia) was

528 used for DNA extraction. Bacterial genomic DNA was tested for purity as previously described for phage DNA

529 and vacuum dried into a pellet for transport. Sequencing was performed using the Illumina® HiSeq 150 bp

530 paired-end platform at the Genewiz® facilities (Suzhou, China).

531 The genomes of AB900, A9844 and their phage-resistant counterparts, were independently assembled

532 from the paired-end 150 nt Illumina reads. Adapter sequences were clipped using Trimmomatic v0.39 (60) in

533 palindrome mode, with quality filtering, quality trimming and length filtering (AVGQUAL:35

534 SLIDINGWINDOW:5:28 MINLEN:80). Trimming outcomes were checked in trimviz

535 (github.com/MonashBioinformaticsPlatform/trimviz). Reads were assembled using Spades v3.12.0 (67) with a

536 coverage cutoff of 10 in 'careful' mode. To identify variants, the filtered sequencing data was mapped back onto

537 the assemblies using BWA (68) as implemented in RNAsik v1.5.0 (69). Both phage-sensitive (S) and phage-

538 resistant (R) sequencing data was mapped back onto each of the genome assemblies from S and R isolates,

539 resulting in 4 alignment files per strain pair (S on S; S on R; R on S; and R on R). Pileup files were generated

540 using samtools mpileup v1.8 and processed using Varscan2 v2.4.0 (70) in both "pileup2snp" and "pileup2indel"

541 modes. Candidate variants (several thousand per alignment) were then filtered using a custom Python script

542 for: 1) contig length > 500 nt; 2) contig coverage in the Spades assembly > 50; 3) realignment coverage > 30

543 reads at the variant site; 4) if the variant is also detected in the self-alignment (S on S) its frequency (proportion

544 of supporting reads vs total overlapping reads) must be at least 25% higher in the non-self-alignment (R on S).

545 Surviving variants were few enough in number to be manually verified. R on S alignments around candidate

546 variants were viewed in IGV v2.3.59 (71) together with the .gff3 annotation files generated by Prokka v.1.13.7

547 (72) to check for coding-region disruptions, and compared to the self-alignment (S on S) to check for alignment

548 artefacts. The reciprocal alignments (S on R, checking R on R for alignment artefacts) were also verified in the

549 homologous region of the R assembly.

550 To infer overall sequence-based relationships between the strains in this study, the publicly available

551 genome assemblies were downloaded (Table S3). For strain AYP A22, however, only raw sequencing data was

552 available, so this was trimmed and assembled as above (Trimmomatic parameters were adjusted to

553 AVGQUAL:28 SLIDINGWINDOW:5:23 MINLEN:40 without adapter-trimming). All assemblies were *de novo*

554 annotated using Prokka and core-genome alignments of coding regions common to all the strains were created

16

555 using Roary v3.11.2 (73). Alignments were converted to PHYLIP format and fed into RAXML v8.2.12 (74) (with

556 the GTRCAT substitution model). To illustrate the relationships between the strains documented in Figure 1,

557 the data was visualized using the R package APE v5.3 (75).

558 **Gene knockout and complementation.** All PCR reactions mentioned in this section were performed

559 using KAPA HiFi DNA Polymerase (Hot Start and Ready Mix formulation) (Roche, Switzerland). Genes of

560 interest were disrupted using a variation of the methods described previously (76). Briefly, ~1000 bp upstream

561 and downstream of the target genes were PCR-amplified from genomic DNA. The kanamycin resistance

562 cassette was amplified from pKD4 (76), and three products combined by splice overlap PCR using primers

563 specified in Table S4. The linear constructs were gel purified using a PCR cleanup kit (Sigma-Aldrich, Australia),

564 confirmed by Sanger sequencing and concentrated to ~500 ng/μl.

565 *A. baumannii* cells were made electrocompetent as follows. Overnight cultures were diluted 1:20 and

566 allowed to grow to an OD_{600} of 0.7. A volume of 5 ml of culture per transformation was pelleted by centrifugation,

567 the cells were washed 3 times in 10% (v/v) glycerol and finally resuspended in 10% glycerol. The cell suspension

568 was mixed with recombinant DNA (~3 μg) and incubated at room temperature for 15 min. The mixture was

569 transferred to a sterile 2 mm electroporation cuvette (Biorad, Australia) and immediately pulsed with a Bio-Rad

570 Micropulser (EC3, 3.0 kV). Pre-warmed (37 °C) Super Optimal Broth (SOB) was immediately added and the

571 cells were transferred to a new tube. The cells were recovered for 3 hours rotating at 37 °C. The recovered cells

572 were pelleted, resuspended in SOB, and spread-plated onto LB agar with and without 50 μg/ml of kanamycin.

573 Isolated colonies from the transformation were patch-plated on LB agar containing 50 μg/ml of kanamycin for

574 two successive re-streaks to ensure kanamycin resistance. Colonies of the knockout mutants were PCR-

575 amplified with the primers on Table S4, ran on a 0.7% agarose gel, and the bands were gel-purified and Sanger-

576 sequenced in order to identify the successful disruption of genes of interest via the insertion of the kanamycin

577 resistance cassette.

578 For complementing the genes of interest back into the knockout mutants, the genes were PCR-amplified

579 using primers containing cut sites for the restriction enzymes *EcoR*I (forward) and *Sal*I (reverse) (New England

580 Biolabs, NEB, Australia) for *gtr29,* or *Sal*I exclusively in the case of *gpi*. Next, two overnight double-digestions

581 were set up at 37 °C for the plasmid pBAD18Kan-Ori (77) and the genes of interest using the restriction

582 enzymes. The digested products were run on a 0.7% agarose gel, excised, purified and ligated for 2 h at room

583 temperature using the Instant Sticky-end Ligase Master Mix (NEB, Australia) following the manufacturer's

584 protocol. The ligated product was then chemically transformed into *Escherichia coli* DH5-α competent cells

585 (NEB, Australia) following the company's protocol. The transformed colonies were patch-plated onto

586 kanamycin-LB plates (50 μg/ml), and confirmed via Sanger sequencing. These confirmed colonies underwent

587 plasmid prep using the GenElute™ Plasmid Miniprep Kit (Sigma-Aldrich, Australia) and the complement-

588 containing plasmid was electroporated into the knockout mutant as per the protocol above.

589 **Capsule quantification and observation.** Quantification of surface polysaccharides was performed

590 following the published protocol of the sulfuric acid-phenol reaction (39). For qualitative observation of capsule

591 thickness, a Maneval's capsule stain was performed using a bacterial colony mixed with one drop of Congo

592 Red (1% aqueous) on a clean glass slide. After drying, the slide was flooded with Maneval's modified stain for

593 1 min, washed with water and blotted dry. Slides were observed using light microscopy under oil immersion.

594 For scanning electron microscopy (SEM) imaging of the surface of bacterial hosts, a 20 μl droplet of 5 times-

595 PBS washed bacterial suspension was placed onto a fresh gold-coated silicon wafer (5 x 5 mm) and the cells

596 allowed to settle for 5 min, followed by washing with PBS. The wafer was then placed in 2.5% glutaraldehyde

597 in PBS solution for 15 min, washed with deionized water and dehydrated by immersing in increasing

598 concentrations of ethanol for 3 minutes each. Residual ethanol was removed with a critical point dryer CPD 030

599 (BAL-TEC AG, Liechtenstein). The sample was mounted on a standard metal SEM stub and then coated with

600 a ~10 nm thick gold layer using a sputter coater SCD 005 (BAL-TEC AG, Liechtenstein). The samples were

601 examined under high vacuum within the FE-SEM ThermoFisher Elstar G4 at an accelerating voltage of 2 kV,

602 secondary electron mode (SE), and a working distance of 4 mm, operating in immersion mode with the through

603 lens detector (TLD).

604 **Biofilm formation assay.** 48 h biofilm formation on polystyrene 96-well plates was assessed using

605 crystal violet staining and spectrophotometry as previously described (78).

606 **Serum killing assay.** From overnight cultures of the strains, a 1:100 subculture was made and

607 incubated to reach mid-exponential phase (approximately 2-3 h). Meanwhile, the working volume of human

608 serum (Sigma-Aldrich, Australia) was divided in half, storing one half at 4 ºC and heat-inactivating the other half

609 at 56 ºC for 30 min. After incubation, the cells of each culture were harvested via centrifugation, washed, and

610 resuspended in PBS, then standardized to an OD_{600} of 0.3. Active or heat-inactivated human serum was then

611 diluted in PBS to a 50% solution. In a glass test tube, 50% serum/PBS was inoculated with 10^5 CFU of bacteria,

612 mixed and incubated. At regular intervals, samples from each culture were extracted to perform serial dilutions

613 and CFU counts. *E. coli* DH5-α was used as a control of serum activity, as it is highly susceptible to human

614 serum but resistant to heat-inactivated serum.

615 **Antibiotic susceptibility assay.** Minimum inhibitory concentrations (MICs) of 7 antibiotics were

616 assessed using the microbroth dilution protocol, as previously described (79) and interpreted using the cut-off

617 values from the Clinical and Laboratory Standard Institute. The antibiotics used were: ampicillin/sulbactam

618 (SAM), ceftazidime (CFZ), imipenem (IPM), gentamicin (GEN), amikacin (AMK), minocycline (MIN), and

619 ciprofloxacin (CIP) (Sigma-Aldrich, Australia). Size of the bacterial inoculum for each test was standardized at

620 10^5 CFU, in a volume of 200 μl per test. *E. coli* strains ATCC 25922 and ATCC 35218 were used as quality

621 controls for each batch of microbroth dilution tests.

622 **Animal experiments and animal ethics.** Four female, 6-to-10 weeks old, BALB/c mice per group were

623 used. Bacterial inoculums of either wild type or phage-resistant *A. baumannii* were prepared to a concentration

624 of 10^6 CFU in 100 μl of PBS. Before administration, the bacterial suspensions were mixed in a 1:1 ratio with 6%

625 porcine stomach mucin (Sigma-Aldrich, Australia) in PBS, for a total volume of 200 μl. Mice were injected

626 intraperitoneally and followed for up to 8 h. At the humane endpoint, blood was extracted through cardiac

627 puncture and a laparotomy was performed to obtain a section of the liver, the right kidney, and spleen. The

628 organs were weighed and then homogenized in PBS. Blood and organ suspensions were then serially diluted

629 in PBS (from 10^{-1} to 10^{-5}) and the bacterial burden quantified by CFU counting, and normalized by organ weight.

630 All protocols involving animals were reviewed and approved by the Monash University Animal Ethics Committee

631 (Project ID: E/1689/2016/M) and complied with the National Health and Medical Research Council guidelines.

632 Animals were housed at the Monash Animal Research Facility, Monash University.

633 **Graphing and statistics.** Graphing and statistical analyses were performed with GraphPad Prism 7

634 (GraphPad Software, Inc.). All *in vitro* experiments were performed in triplicate, with at least two technical

635 replicates each. Where appropriate, scatter plots and medians were presented (80). Both parametric and

636 nonparametric statistical analyses were performed, and the threshold value of two-tailed $p < 0.05$ used for

637 statistical significance.

638

Acknowledgements

Author Contributions

Conceptualization: FGA, TJL, AYP, JJB; Methodology: FGA, JHF, RP, XK, MT, SA, FM, DK, JJB; Formal Analysis: SA; Investigation: FGA, JHF, RP, XK, MT, DS, CO, LK, DK; Resources: MKO'B, TJL, AYP, JJB; Writing – Original Draft Preparation: FGA, JJB; Writing – Review and Editing: FGA, JHF, RP, XK, MT, DS, SA, FM, CO, LK, DK, MKO'B, TJL, AYP, JJB; Supervision and Funding Acquisition: TJL, AYP, JJB.

References

1. World Health Organization. Ten threats to global health in 2019 [internet]. Geneva: World Health Organization; 2019 [cited 11 January 2020] Available from: https://www.who.int/emergencies/ten-threats-to-global-health-in-2019.

2. Cosgrove SE. The relationship between antimicrobial resistance and patient outcomes: mortality, length of hospital stay, and health care costs. *Clin Infect Dis.* 2006;42(Suppl2):S82-S89.

3. Naylor NR, Atun R, Zhu N, Kulasabanathan K, Silva S, Chatterjee A, et al. Estimating the burden of antimicrobial resistance: a systematic literature review. *Antimicrob Resist Infect Control*. 2018;7:58.

4. Centers for Disease Control and Prevention. Antibiotic resistance threats in the United States [internet]. Atlanta, GA, USA: Department of Health and Human Services CDC; 2019 [cited 11 January 2020] Available from: https://www.cdc.gov/drugresistance/Biggest-Threats.html

5. World Health Organization. Global priority list of antibiotic-resistant bacteria to guide research, discovery, and development of new antibiotics [internet]. Geneva: World Health Organization; 2017 p. 5. Available from: https://www.who.int/medicines/publications/WHO-PPL-Short_Summary_25Feb-ET_NM_WHO.pdf

6. Pendleton JN, Gorman SP, Gilmore BF. Clinical relevance of the ESKAPE pathogens. *Expert Rev Anti Infect Ther*. 2013;11:297-308.

7. Chapartegui-González I, Lázaro-Díez M, Bravo Z, Navas J, Icardo JM, Ramos-Vivas J. *Acinetobacter baumannii* maintains its virulence after long-time starvation. *PloS one*. 2018;13:e0201961.

8. Peleg AY, Seifert H, Paterson DL. *Acinetobacter baumannii*: emergence of a successful pathogen. *Clin Microbiol Reviews*. 2008;21:538-582.

9. Vincent JL, Rello J, Marshall J, Silva E, Anzueto A, Martin CD, et al. International study of the prevalence and outcomes of infection in intensive care units. *JAMA*. 2009;302:2323-2329.

10. Morris FC, Dexter C, Kostoulias X, Uddin MI, Peleg AY. The mechanisms of disease caused by *Acinetobacter baumannii*. *Front Microbiol*. 2019;10:1601.

11. Geisinger E, Huo W, Hernandez-Bird J, Isberg RR. *Acinetobacter baumannii*: envelope determinants that control drug resistance, virulence, and surface variability. *Annu Rev Microbiol*. 2019;73:481-506.

12. Salwiczek M, Qu Y, Gardiner J, Strugnell RA, Lithgow T, McLean KM, et al. Emerging rules for effective antimicrobial coatings. *Trends Biotechnol*. 2014;32:82-90.

13. Davenport EK, Call DR, Beyenal H. Differential protection from tobramycin by extracellular polymeric substances from *Acinetobacter baumannii* and *Staphylococcus aureus* biofilms. *Antimicrob Agents Chemother*. 2014;58:4755-4761.

14. Longo F, Vuotto C, Donelli G. Biofilm formation in *Acinetobacter baumannii*. *New Microbiol*. 2014;37:119-127.

685   15. Ryu SY, Baek W-K, Kim HA. Association of biofilm production with colonization among clinical isolates of
686   *Acinetobacter baumannii*. *Korean J Intern Med*. 2017;32:345-351.

687   16. Singh JK, Adams FG, Brown MH. Diversity and function of capsular polysaccharide in *Acinetobacter baumannii*. *Front*
688   *Microbiol*. 2019;9:3301.

689   17. Gordillo Altamirano FL, Barr JJ. Phage therapy in the postantibiotic era. *Clin Microbiol Rev*. 2019;32:e00066-18.

690   18. Viertel TM, Ritter K, Horz H-P. Viruses versus bacteria—novel approaches to phage therapy as a tool against
691   multidrug-resistant pathogens. *J Antimicrob Chemother*. 2014;69:2326-2336.

692   19. Hua Y, Luo T, Yang Y, Dong D, Wang R, Wang Y, et al. Phage therapy as a promising new treatment for lung
693   infection caused by carbapenem-resistant *Acinetobacter baumannii* in mice. *Front Microbiol*. 2017;8:2659.

694   20. Wang JL, Kuo CF, Yeh CM, Chen JR, Cheng MF, Hung CH. Efficacy of phikm18p phage therapy in a murine model
695   of extensively drug-resistant *Acinetobacter baumannii* infection. *Infect Drug Resist*. 2018;11:2301-2310.

696   21. Yin S, Huang G, Zhang Y, Jiang B, Yang Z, Dong Z, et al. Phage Abp1 rescues human cells and mice from infection
697   by pan-drug resistant *Acinetobacter baumannii*. *Cell Physiol Biochem*. 2017;44:2337-2345.

698   22. Schooley RT, Biswas B, Gill JJ, Hernandez-Morales A, Lancaster J, Lessor L, et al. Development and use of
699   personalized bacteriophage-based therapeutic cocktails to treat a patient with a disseminated resistant *Acinetobacter*
700   *baumannii* infection. *Antimicrob Agents Chemother*. 2017;61:e00954-17.

701   23. Wyres KL, Cahill SM, Holt KE, Hall RM, Kenyon JJ. Identification of *Acinetobacter baumannii* loci for capsular
702   polysaccharide (KL) and lipooligosaccharide outer core (OCL) synthesis in genome assemblies using curated
703   reference databases compatible with Kaptive. *bioRxiv*. 2019:869370.

704   24. Golkar Z, Bagasra O, Pace DG. Bacteriophage therapy: a potential solution for the antibiotic resistance crisis. *J Infect*
705   *Dev Ctries*. 2014;8:129-136.

706   25. Labrie SJ, Samson JE, Moineau S. Bacteriophage resistance mechanisms. *Nature Rev Microbiol*. 2010;8:317-327.

707   26. Torres-Barcelo C, Hochberg ME. Evolutionary rationale for phages as complements of antibiotics. *Trends Microbiol*.
708   2016;24:249-256.

709   27. León M, Bastías R. Virulence reduction in bacteriophage resistant bacteria. *Front Microbiol*. 2015;6:343.

710   28. Capparelli R, Nocerino N, Lanzetta R, Silipo A, Amoresano A, Giangrande C, et al. Bacteriophage-resistant
711   *Staphylococcus aureus* mutant confers broad immunity against staphylococcal infection in mice. *PLoS One*.
712   2010;5:e11720.

713   29. Capparelli R, Nocerino N, Iannaccone M, Ercolini D, Parlato M, Chiara M, et al. Bacteriophage therapy of *Salmonella*
714   *enterica*: a fresh appraisal of bacteriophage therapy. *J Infect Dis*. 2010;201:52-61.

715   30. Chan BK, Sistrom M, Wertz JE, Kortright KE, Narayan D, Turner PE. Phage selection restores antibiotic sensitivity in
716   MDR *Pseudomonas aeruginosa*. *Sci Rep*. 2016;6:26717.

717   31. Adams MD, Goglin K, Molyneaux N, Hujer KM, Lavender H, Jamison JJ, et al. Comparative genome sequence
718   analysis of multidrug-resistant *Acinetobacter baumannii*. *J Bacteriol*. 2008;190:8053-8064.

719   32. Hawkey J, Ascher DB, Judd LM, Wick RR, Kostoulias X, Cleland H, et al. Evolution of carbapenem resistance in
720   *Acinetobacter baumannii* during a prolonged infection. *Microbial Genom*. 2018;4. doi: 10.1099/mgen.0.000165.

721   33. Peleg AY, Tampakakis E, Fuchs BB, Eliopoulos GM, Moellering RC, Mylonakis E. Prokaryote–eukaryote interactions
722   identified by using *Caenorhabditis elegans*. *Proc Natl Acad Sci USA*. 2008;105:14585-14590.

723   34. Jacobs AC, Thompson MG, Black CC, Kessler JL, Clark LP, McQueary CN, et al. AB5075, a highly virulent isolate of
724   *Acinetobacter baumannii*, as a model strain for the evaluation of pathogenesis and antimicrobial treatments. *mBio*.
725   2014;5:e01076-14.

726   35. Schaub IG, Hauber FD. A Biochemical and serological study of a group of identical unidentifiable gram-negative
727   bacilli from human sources. *J Bacteriol*. 1948;56:379-385.

728   36. Bonilla N, Rojas MI, Netto Flores Cruz G, Hung S-H, Rohwer F, Barr JJ. Phage on tap–a quick and efficient protocol
729   for the preparation of bacteriophage laboratory stocks. *PeerJ*. 2016;4:e2261.

730   37. Kieft K, Zhou Z, Anantharaman K. VIBRANT: Automated recovery, annotation and curation of microbial viruses, and
731   evaluation of virome function from genomic sequences. *bioRxiv*. 2019:855387.

732 38. Kenyon JJ, Hall RM. Variation in the complex carbohydrate biosynthesis loci of *Acinetobacter baumannii* genomes.
733   *PLoS One*. 2013;8:e62160.

734 39. Brimacombe C, Beatty J. Surface polysaccharide extraction and quantification. *Bio Protoc*. 2013;3:e934.

735 40. Russo TA, Luke NR, Beanan JM, Olson R, Sauberan SL, MacDonald U, et al. The K1 capsular polysaccharide of
736   *Acinetobacter baumannii* strain 307-0294 is a major virulence factor. *Infect Immun*. 2010;78:3993-4000.

737 41. Wang-Lin SX, Olson R, Beanan JM, MacDonald U, Balthasar JP, Russo TA. The capsular polysaccharide of
738   *Acinetobacter baumannii* is an obstacle for therapeutic passive immunization strategies. *Infect Immun*.
739   2017;85:e00591-17.

740 42. Oechslin F. Resistance development to bacteriophages occurring during bacteriophage therapy. *Viruses*.
741   2018;10:351.

742 43. Kenyon JJ, Shashkov AS, Senchenkova SyN, Shneider MM, Liu B, Popova AV, et al. *Acinetobacter baumannii* K11
743   and K83 capsular polysaccharides have the same 6-deoxy-l-talose-containing pentasaccharide K units but different
744   linkages between the K units. *Int J Biol Macromol*. 2017;103:648-655.

745 44. Kenyon JJ, Marzaioli AM, Hall RM, De Castro C. Structure of the K2 capsule associated with the KL2 gene cluster of
746   *Acinetobacter baumannii*. *Glycobiology*. 2014;24:554-63.

747 45. Sørensen MCH, van Alphen LB, Harboe A, Li J, Christensen BB, Szymanski CM, et al. Bacteriophage F336
748   recognizes the capsular phosphoramidate modification of *Campylobacter jejuni* NCTC11168. *J Bacteriol*.
749   2011;193:6742-6749.

750 46. Pickard D, Toribio AL, Petty NK, van Tonder A, Yu L, Goulding D, et al. A conserved acetyl esterase domain targets
751   diverse bacteriophages to the Vi capsular receptor of *Salmonella enterica* serovar Typhi. *J Bacteriol*. 2010;192:5746-
752   5754.

753 47. Hsu C-R, Lin T-L, Pan Y-J, Hsieh P-F, Wang J-T. Isolation of a bacteriophage specific for a new capsular type of
754   *Klebsiella pneumoniae* and characterization of its polysaccharide depolymerase. *PLoS One*. 2013;8:e70092.

755 48. Schumacher A, Vranken T, Malhotra A, Arts JJC, Habibovic P. *In vitro* antimicrobial susceptibility testing methods:
756   agar dilution to 3D tissue-engineered models. *Eur J Clin Microbiol Infect Dis*. 2018;37:187-208.

757 49. Humphries JC. Enzymic activity of bacteriophage-culture lysates: I. A capsule lysin active against *Klebsiella*
758   *pneumoniae* type A. *J Bacteriol*. 1948;56:683-693.

759 50. Henderson B, Martin A. Bacterial virulence in the moonlight: multitasking bacterial moonlighting proteins are virulence
760   determinants in infectious disease. *Infect Immun*. 2011;79:3476-3491.

761 51. Boinett CJ, Cain AK, Hawkey J, Do Hoang NT, Khanh NNT, Thanh DP, et al. Clinical and laboratory-induced colistin-
762   resistance mechanisms in *Acinetobacter baumannii*. *Microb Genom*. 2019;5:e000246.

763 52. Zhang P, Wei D, Li Z, Sun Z, Pan J, Zhu X. Cryptococcal phosphoglucose isomerase is required for virulence factor
764   production, cell wall integrity and stress resistance. *FEMS Yeast Res*. 2015;15:fov072.

765 53. Tsuge S, Ochiai H, Inoue Y, Oku T, Tsuno K, Kaku H, et al. Involvement of phosphoglucose isomerase in
766   pathogenicity of *Xanthomonas oryzae* pv. *oryzae*. *Phytopathology*. 2004;94:478-483.

767 54. Lai M-J, Chang K-C, Huang S-W, Luo C-H, Chiou P-Y, Wu C-C, et al. The tail associated protein of *Acinetobacter*
768   *baumannii* phage ΦAB6 Is the host specificity determinant possessing exopolysaccharide depolymerase activity.
769   *PLoS One*. 2016;11:e0153361.

770 55. Popova AV, Lavysh DG, Klimuk EI, Edelstein MV, Bogun AG, Shneider MM, et al. Novel Fri1-like viruses infecting
771   *Acinetobacter baumannii*-vB_AbaP_AS11 and vB_AbaP_AS12-characterization, comparative genomic analysis, and
772   host-recognition strategy. *Viruses*. 2017;9:188.

773 56. Kutter E. Phage host range and efficiency of plating. *Methods Mol Biol*. 2009;501:141-149.

774 57. Davison E, Colquhoun W. Ultrathin formvar support films for transmission electron microscopy. *J Electron Microsc*
775   *Tech*. 1985;2:35-43.

776 58. Dunstan RA, Pickard D, Dougan S, Goulding D, Cormie C, Hardy J, et al. The flagellotropic bacteriophage YSD1
777   targets *Salmonella* Typhi with a Chi-like protein tail fibre. *Mol Microbiol*. 2019;112:1831-1846.

778   59. Wick RR, Judd LM, Holt KE. Deepbinner: Demultiplexing barcoded Oxford Nanopore reads with deep convolutional
779   neural networks. *PLoS Comput Biol*. 2018;14:e1006583.

780   60. Bolger AM, Lohse M, Usadel B. Trimmomatic: a flexible trimmer for Illumina sequence data. *Bioinformatics*.
781   2014;30:2114-2120.

782   61. Wick RR, Judd LM, Gorrie CL, Holt KE. Unicycler: Resolving bacterial genome assemblies from short and long
783   sequencing reads. *PLoS Comput Biol*. 2017;13:e1005595.

784   62. Aziz RK, Bartels D, Best AA, DeJongh M, Disz T, Edwards RA, et al. The RAST Server: rapid annotations using
785   subsystems technology. *BMC Genomics*. 2008;9:75. doi: 10.1186/1471-2164-9-75

786   63. Arndt D, Grant JR, Marcu A, Sajed T, Pon A, Liang Y, et al. PHASTER: a better, faster version of the PHAST phage
787   search tool. *Nucleic Acids Res*. 2016;44(W1):W16-W21.

788   64. Pope W, Sarkis G, Hatfull G, Broussard G. Lysogeny experiments [internet]. Pittsburg, PA, USA: The
789   Actinobacteriophage Database at PhagesDB.org; 2013 [cited 30 January 2020] Available from:
790   https://phagesdb.org/media/workflow/protocols/pdfs/LysogenyProtocol_3.19.13.pdf

791   65. Boling L, Cuevas DA, Grasis JA, Kang HS, Knowles B, Levi K, et al. Dietary prophage inducers and antimicrobials:
792   toward landscaping the human gut microbiome. *Gut Microbes*. 2020;13:1-14.

793   66. Gillis A, Mahillon J. An improved method for rapid generation and screening of *Bacillus thuringiensis* phage-resistant
794   mutants. *J Microbiol Methods*. 2014;106:101-103.

795   67. Nurk S, Bankevich A, Antipov D, Gurevich AA, Korobeynikov A, Lapidus A, et al. Assembling single-cell genomes and
796   mini-metagenomes from chimeric MDA products. *J Comput Biol*. 2013;20:714-737.

797   68. Li H. Aligning sequence reads, clone sequences and assembly contigs with BWA-MEM. *arXiv*. 2013;arXiv:13033997.

798   69. Tsyganov K, James Perry A, Kenneth Archer S, Powell D. RNAsik: A Pipeline for complete and reproducible RNA-seq
799   analysis that runs anywhere with speed and ease. J Open Source Softw. 2018;3:583.

800   70. Koboldt DC, Zhang Q, Larson DE, Shen D, McLellan MD, Lin L, et al. VarScan 2: somatic mutation and copy number
801   alteration discovery in cancer by exome sequencing. *Genome Res*. 2012;22:568-576.

802   71. Robinson JT, Thorvaldsdottir H, Wenger AM, Zehir A, Mesirov JP. Variant review with the integrative genomics
803   viewer. *Cancer Res*. 2017;77:e31-e34.

804   72. Seemann T. Prokka: rapid prokaryotic genome annotation. *Bioinformatics*. 2014;30:2068-2069.

805   73. Page AJ, Cummins CA, Hunt M, Wong VK, Reuter S, Holden MT, et al. Roary: rapid large-scale prokaryote pan
806   genome analysis. *Bioinformatics*. 2015;31:3691-3693.

807   74. Stamatakis A. RAxML version 8: a tool for phylogenetic analysis and post-analysis of large phylogenies.
808   *Bioinformatics*. 2014;30:1312-1313.

809   75. Paradis E, Schliep K. ape 5.0: an environment for modern phylogenetics and evolutionary analyses in R.
810   *Bioinformatics*. 2019;35:526-528.

811   76. Datsenko KA, Wanner BL. One-step inactivation of chromosomal genes in *Escherichia coli* K-12 using PCR products.
812   *Proc Natl Acad Sci*. 2000;97:6640.

813   77. Choi AH, Slamti L, Avci FY, Pier GB, Maira-Litran T. The pgaABCD locus of *Acinetobacter baumannii* encodes the
814   production of poly-beta-1-6-N-acetylglucosamine, which is critical for biofilm formation. *J Bacteriol*. 2009;191:5953-
815   5963.

816   78. O'Toole GA, Pratt LA, Watnick PI, Newman DK, Weaver VB, Kolter R. Genetic approaches to study of biofilms.
817   *Methods Enzymol*. 1999;310:91-109.

818   79. Wiegand I, Hilpert K, Hancock RE. Agar and broth dilution methods to determine the minimal inhibitory concentration
819   (MIC) of antimicrobial substances. *Nat Protoc*. 2008;3:163-175.

820   80. Weissgerber TL, Milic NM, Winham SJ, Garovic VD. Beyond bar and line graphs: time for a new data presentation
821   paradigm. *PLoS Biol*. 2015;13:e1002128.

822

Supplementary Information
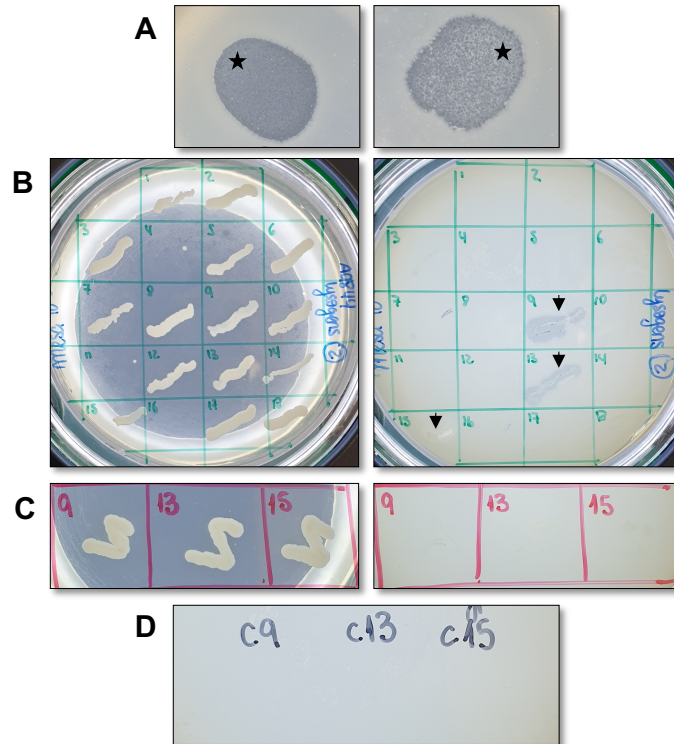
Figure S1. Attempted production of A9844 lysogens. A: Spot assay with droplets containing 10^6 (left) and 10^4 (right) PFU of øCO01 after 48 h of incubation. Black stars denote the zones of lysis containing cloudy bacterial growth. B: Patch assay. Bacterial growth scraped off from the lysis zones was streaked-plated and individual colonies were patched onto LB (left) and LB with an A9844 overlay (right) plates. Black arrows (colonies 9, 13 and 15) show bacterial growth with surrounding lysis, indicating the presence of phage øCO01, possibly released from a lysogen. Panel only shows 18/36 screened colonies. C: After three rounds of single-colony purification, the patch test was repeated for colonies 9, 13 and 15, without indication of phage presence. D: Spot assay performed with the filtered supernatant from cultures of colonies 9, 13 and 15, with no indication of spontaneous phage release.
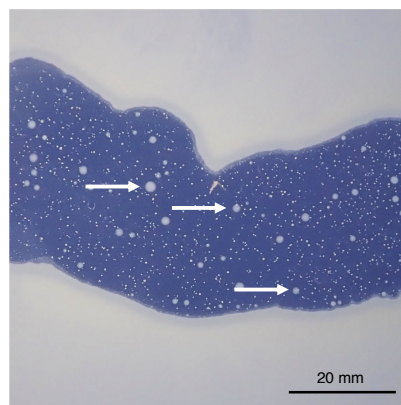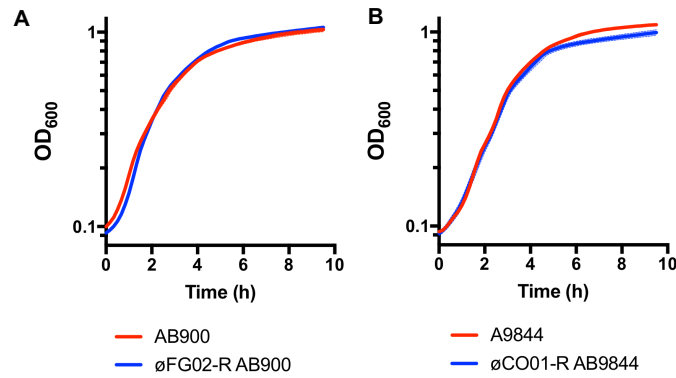

Figure S2. Spot assay of strain A9844 with phage øCO01, showing the large central lysis zone, with several bacterial colonies growing within (white arrowheads). These colonies were assumed to be phage-resistant and underwent the pipeline for confirming this phenotype.
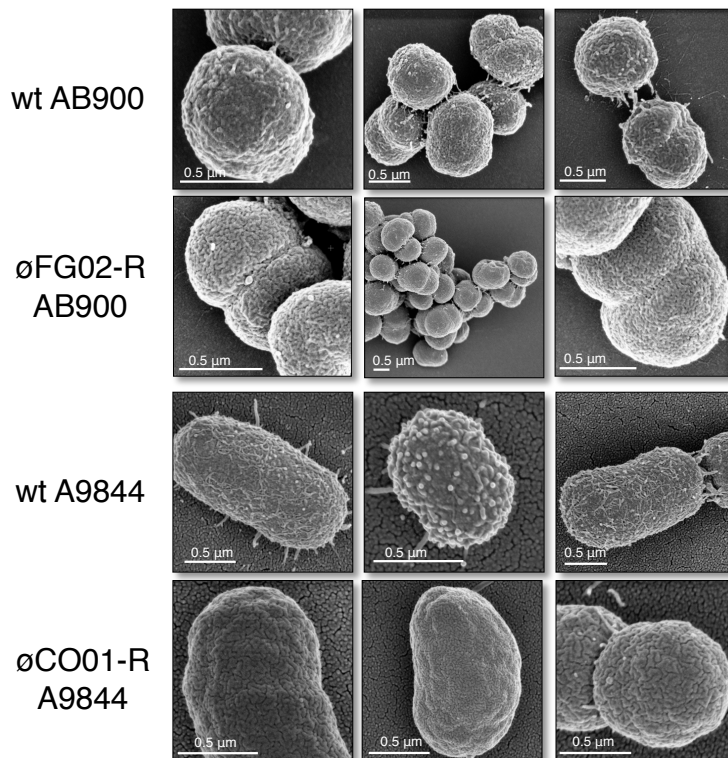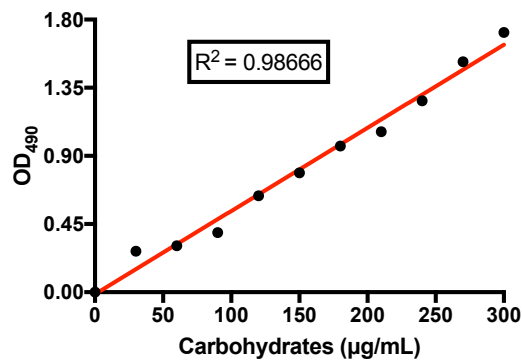
23

Figure S3. Growth curves of A. baumannii strains AB900 and A9844 (red) and their phage-resistant mutants øFG02-R AB900 and øCO01-R A9844 (blue) in the absence of phages. Shaded zones represent SD (n = 3).

Figure S4. Additional scanning electron microscopy images of the wild type and phage-resistant strains in this study.

Figure S5. Standard curve for the capsule quantification assay. Carbohydrate standards were prepared by diluting a carbohydrate stock solution (50:50 mixture of 0.5 mg/ml each of sucrose and fructose) into 1 ml aliquots ranging from 0 to 300 µg/ml of carbohydrate using distilled water. The standards were treated with the phenol-chloroform reaction, and the absorbance measured at OD_{490}.

24

850 **Table S1.** Raw data of minimum inhibitory concentrations (MIC) in μg/ml from the antibiotic resistance panel of

851 AB900, A9844, øFG02-R AB900 and øCO01-R A9844. MICs determined via the microbroth dilution method.

852

	AB900			øFG02-R AB900		
	Replicates			Replicates		
	1	2	3	1	2	3
Ampicillin + Sulbactam	2/1	8/4	4/2	2/1	4/2	2/1
Ceftazidime	>32	>32	8	2	2	1
Imipenem	0.12	0.12	0.25	≤0.06	≤0.06	0.25
Ciprofloxacin	0.5	0.25	0.25	0.25	0.12	0.25
Amikacin	2	1	4	≤0.25	1	4
Gentamicin	0.5	0.5	1	0.5	0.5	0.5
Minocycline	≤0.12	≤0.12	0.25	≤0.12	≤0.12	0.25
	A9844			øCO01-R A9844		
	Replicates			Replicates		
	1	2	3	1	2	3
Ampicillin + Sulbactam	16/8	16/8	16/8	8/4	8/4	16/8
Ceftazidime	>16	64	64	>16	32	64
Imipenem	8	>32	32	8	16	32
Ciprofloxacin	>8	>8	>8	>8	>8	>8
Amikacin	0.25	≤0.25	2	0.5	2	0.25
Gentamicin	2	1	0.5	2	0.5	2
Minocycline	2	2	2	2	1	1

853
854

25

Table S2. Strains and plasmids used in this study

Name	Description/Use	Reference / Source
Acinetobacter baumannii strains		
AB900	Wild type, sensitive to øFG02	(31)
øFG02-R AB900	Obtained *in vitro,* resistant to øFG02	This study
∆gtr29 AB900	Disruption of gene *gtr29*, resistant to øFG02	This study
∆gtr29 (pBAD19) AB900	Complemented AB900 *gtr29* mutant, with *gtr29* supplied *in trans* (pBAD19)	This study
A9844	Wild type, sensitive to øCO01	(33)
øCO01-R A9844	Obtained *in vitro,* resistant to øCO01	This study
∆gpi A9844	Disruption of gene *gpi*, resistant to øCO01	This study
∆gpi (pBAD20) A9844	Complemented A9844 *gpi* mutant, with *gpi* supplied *in trans* (pBAD20)	This study
ATCC 19606	Reference strain, originally from a urinary tract infection.	(35)
ATCC 17978	Reference strain, originally from a case of spinal meningitis.	(31)
AB5075	Clinical strain, from an osteomyelitis case.	(34)
AB307-0294	Clinical strain, from a bloodstream infection.	(31)
APA1	Clinical strain, from a burn wound infection.	(32)
APA2	Clinical strain, from a burn wound infection.	(32)
AYP A22	Clinical strain, from a burn wound infection.	(32)
Escherichia coli strains		
DH5-α	Receptor for production of plasmids pBAD19 and pBAD20; control for complement system activity in serum killing assay.	Commercial
ATCC 25922	Quality control in microbroth dilution antibiotic sensitivity tests.	Commercial
ATCC 35218	Quality control in microbroth dilution antibiotic sensitivity tests.	Commercial
Enterococcus faecium strains		
ATCC 29212	Growth control on inverted spot assays.	Commercial
Plasmids		
pKD4	Source of the kanamycin-resistance cassette.	(76)
pBAD18Kan-Ori	Shuttle vector containing ABori for replication in *A. baumannii*, with araBAD promoter	(77)
pBAD19	pBAD18Kan-Ori with a copy of *gtr29* from AB900, cloned in between *EcoR*I and *Sal*I restriction sites, under control of promoter araBAD.	This study
pBAD20	pBAD18Kan-Ori with a copy of *gpi* from A9844, cloned in at *Sal*I restriction sites, under control of promoter araBAD.	This study

859
860

Table S3. Genome assembly sources for the phylogenetic analysis of *A. baumannii* strains.

Strain	Source
AB900	De novo assembly, from this study; and ftp://ftp.ncbi.nlm.nih.gov/genomes/all/GCA/000/173/395/GCA_000173395.1_ASM17339v1/GCA_000173395.1_ASM17339v1_genomic.fna.gz
A9844	De novo assembly, from this study.
ATCC 19606	ftp://ftp.ncbi.nlm.nih.gov/genomes/all/GCA/000/737/145/GCA_000737145.1_ASM73714v1/GCA_000737145.1_ASM73714v1_genomic.fna.gz
ATCC 17978	ftp://ftp.ncbi.nlm.nih.gov/genomes/all/GCA/001/077/675/GCA_001077675.1_ASM107767v1/GCA_001077675.1_ASM107767v1_genomic.fna.gz
AB5075	ftp.ncbi.nlm.nih.gov/genomes/all/GCF/000/963/815/GCF_000963815.1_ASM96381v1/GCF_000963815.1_ASM96381v1_genomic.fna.gz
AB307-0294	ftp://ftp.ncbi.nlm.nih.gov/genomes/all/GCA/002/803/025/GCA_002803025.1_ASM280302v1/GCA_002803025.1_ASM280302v1_genomic.fna.gz
APA1	https://ndownloader.figshare.com/files/9042523
APA2	https://ndownloader.figshare.com/files/9042526
AYP A22	No assembly. Downloaded raw sequencing data from SRA, accession: SRR5891477

861
862

863 **Table S4.** Primers used in the genetic engineering of *A. baumannii* strains AB900 and A9844 in this study. '/'

864 indicates the addition of an extension sequence.

Number	Name	Use	Sequence (5'-3')
		Construct for knocking out gtr29 in AB900	
1	UPgtr29-FWD	Upstream region of gtr29	GCTTCTTCTCGTTCAATATATGG
2	UPgtr29-RVS	Upstream region of gtr29 / Extension with homology to KAN-FWD	CCCAGTAGCTGACATTCATCC / GTAGAATATACGAACACATTGAG
3	KAN-FWD	Amplification of the kanamycin resistance cassette from plasmid vector pKD4 (also used for the other construct)	GGATGAATGTCAGCTACTGGG
4	KAN-RVS		GAATCGAAATCTCGTGATGGCAG
5	DWNgtr29-FWD	Downstream region of gtr29 / Extension with homology to KAN-RVS	CTGCCATCACGAGATTTCGATTC / GCTCAATTGATGGATGGTTAG
6	DWNgtr29-RVS	Downstream region of gtr29	GGAATTGACTTACTTGCTGGTAG
7	NESgtr29-FWD	Nested primers for amplification of the final construct	GTTGTTTATCCGACTCAGAG
8	NESgtr29-RVS		CAAACCAGCAACAGGTAAAATGG
9	SEQgtr29-FWD	Confirmation of gene disruption via Sanger sequencing	GTTAATCGTGGTGAAGTTGTAC
10	SEQgtr29-RVS		GATACGCATGCATTCTAACAGG
		Construct for knocking out gpi in A9844	
11	UPgpi-FWD	Upstream region of gpi	ACTATGCAAGAGCTGTTACGTCC
12	UPgpi-RVS	Upstream region of gpi / Extension with homology to KAN-FWD	CCCAGTAGCTGACATTCATCC / ATAAGCGCTCAATCCAGTGAGTC
13	DWNgpi-FWD	Downstream region of gpi / Extension with homology to KAN-RVS	CTGCCATCACGAGATTTCGATTC / ATGCTTCAACACGTGGTTTGATT
14	DWNgpi-RVS	Downstream region of gpi	CAGCTATCCTTAAGCATATCTTC
15	NESgpi-FWD	Nested primers for amplification of the final construct	GCTGAATTTACAAAGCTCAGCA
16	NESgpi-RVS		TGCTCTACGTGGAGCGAACTCA
17	SEQgpi-FWD	Confirmation of gene disruption via Sanger sequencing	CGCTTATGAAGGAGTAGGTC
18	SEQgpi-RVS		TGCTCTCGAAACACTCGGTC
		Plasmid complementation of gtr29	
19	UPgtr29-ECORI-FWD	Buffer zone / EcoRI recognition sequence / Upstream region of gtr29 (primer 1)	AGACAC / GAATTC / GCTTCTTCTCGTTCAATATATGG
20	DWNgtr29-SalI-RVS	Buffer zone / SalI recognition sequence / Downstream region of gtr29 (primer 6)	AGATCA / GTCGAC / GGAATTGACTTACTTGCTGGTAG
21	pBAD19-MCS-FWD	Confirmation of plasmid-complemented colonies	GATTAGCGGATCCTACCTGACG
22	pBAD19-MCS-RVS		CACTTCTGAGTTCGGCATGG
		Plasmid complementation of gpi	
23	UPgpi-SalI-FWD	Buffer zone / SalI recognition sequence / Upstream region of gpi (primer 11)	AGATCA / GTCGAC / ACTATGCAAGAGCTGTTACGTCC
24	DWNgpi-SalI-RVS	Buffer zone / SalI recognition sequence / Downstream region of gpi (primer 14)	AGATCA / GTCGAC / CAGCTATCCTTAAGCATATCTTC
25	pBAD20-MCS-FWD	Confirmation of plasmid-complemented colonies	GATTAGCGGATCCTACCTGACG
26	pBAD20-MCS-RVS		CACTTCTGAGTTCGGCATGG

865

866

28